Cell Reports

Article

Targeting EphA2 suppresses hepatocellular carcinoma initiation and progression by dual inhibition of JAK1/STAT3 and AKT signaling

Graphical Abstract

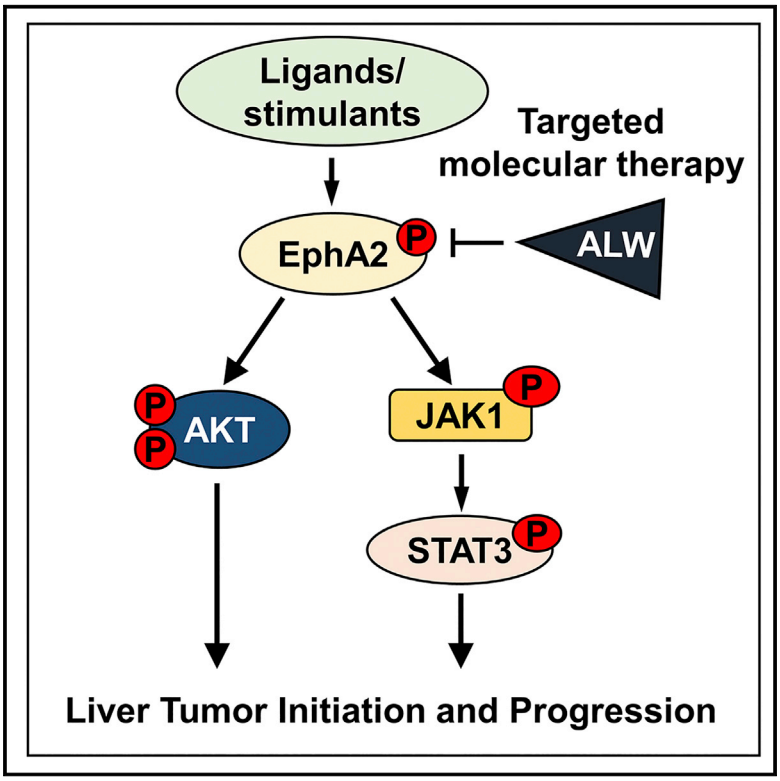

Authors

Hao Wang, Wei Hou, Aldeb Perera, ..., Fowsiyo Ahmed, Lewis R. Roberts, Wei Qiu

Correspondence

wqiu@luc.edu

In brief

Wang et al. define the role of receptor tyrosine kinase EphA2 in the development of hepatocellular carcinoma and elucidate its mechanisms of action. Inhibition of EphA2 is a promising strategy for the treatment of advanced hepatocellular carcinoma.

Highlights

- High EphA2 signaling is associated with worse clinical outcomes in HCC patients
- Inhibition of EphA2 suppresses HCC growth both *in vitro* and *in vivo*
- EphA2 promotes hepatocarcinogenesis by dual activation of AKT and JAK1/STAT3 signaling
- EphA2 inhibitor ALW-II-41-27 suppresses HCC growth

Wang et al., 2021, Cell Reports *34*, 108765
February 23, 2021 © 2021 The Authors.
https://doi.org/10.1016/j.celrep.2021.108765

CellPress

Cell Reports

CellPress
OPEN ACCESS

Article

Targeting EphA2 suppresses hepatocellular carcinoma initiation and progression by dual inhibition of JAK1/STAT3 and AKT signaling

Hao Wang,[1,2] Wei Hou,[1,2] Aldeb Perera,[1,2] Carlee Bettler,[1,2] Jordan R. Beach,[3] Xianzhong Ding,[4] Jun Li,[5] Mitchell F. Denning,[2] Asha Dhanarajan,[6] Scott J. Cotler,[6] Cara Joyce,[7] Jun Yin,[8] Fowsiyo Ahmed,[8] Lewis R. Roberts,[8] and Wei Qiu[1,2,9,*]

[1]Department of Surgery, Loyola University Chicago Stritch School of Medicine, Maywood, IL, USA
[2]Department of Cancer Biology, Loyola University Chicago Stritch School of Medicine, Maywood, IL, USA
[3]Department of Cell and Molecular Physiology, Loyola University Chicago Stritch School of Medicine, Maywood, IL, USA
[4]Department of Pathology, Loyola University Chicago Stritch School of Medicine, Maywood, IL, USA
[5]Department of Applied and Computational Mathematics and Statistics, University of Notre Dame, Notre Dame, IN, USA
[6]Department of Medicine, Loyola University Chicago Stritch School of Medicine, Maywood, IL, USA
[7]Department of Public Health Sciences, Loyola University Chicago Stritch School of Medicine, Maywood, IL, USA
[8]Department of Medicine, Mayo Clinic, Rochester, MN, USA
[9]Lead contact
*Correspondence: wqiu@luc.edu
https://doi.org/10.1016/j.celrep.2021.108765

SUMMARY

Hepatocellular carcinoma (HCC) remains one of the deadliest malignancies worldwide. One major obstacle to treatment is a lack of effective molecular-targeted therapies. In this study, we find that EphA2 expression and signaling are enriched in human HCC and associated with poor prognosis. Loss of EphA2 suppresses the initiation and growth of HCC both *in vitro* and *in vivo*. Furthermore, CRISPR/CAS9-mediated EphA2 inhibition significantly delays tumor development in a genetically engineered murine model of HCC. Mechanistically, we discover that targeting EphA2 suppresses both AKT and JAK1/STAT3 signaling, two separate oncogenic pathways in HCC. We also identify a small molecule kinase inhibitor of EphA2 that suppresses tumor progression in a murine HCC model. Together, our results suggest EphA2 as a promising therapeutic target for HCC.

INTRODUCTION

Hepatocellular carcinoma (HCC) accounts for 90% of all primary liver cancers worldwide (Ferlay et al., 2015). Liver cancer is the sixth most common cancer, and the fourth most common cause of cancer death worldwide (Villanueva, 2019). The prognosis for patients with HCC is poor, with a 5-year survival of 18% (Villanueva, 2019). The Food and Drug Administration (FDA) approved the VEGFR inhibitor sorafenib as a first-line treatment for advanced HCC in 2008. Sorafenib provides limited clinical benefit, increasing overall survival (OS) by 2.8 months compared to placebo, and achieving an overall response rate of less than 2% (Llovet et al., 2008). In recent years, additional molecular agents such as the first-line treatment lenvatinib, second-line treatments regorafenib, cabozantinib, and checkpoint inhibitors nivolumab and pembrolizumab have been approved by the FDA. However, all are marked by low response rates and limited overall survival benefit. Recently, atezolizumab, combined with bevacizumab, showed better overall and progression-free survival outcomes than sorafenib in patients with unresectable hepatocellular carcinoma (Finn et al., 2020). The exciting results led to the approval of this combination as the first-line treatment by the FDA for HCC patients. However, 58.6% of patients receiving atezolizumab-bevacizumab still had disease progression or died within 12 months after the treatment (Finn et al., 2020).

A significant challenge in drug development is that HCC has the fewest somatic mutations among solid tumors that can be targeted pharmacologically (Villanueva, 2019). The majority of approved therapies for advanced HCC primarily targets VEGFR, which targets the tumor vasculature but not the crucial oncodrivers directly. Available treatments could benefit patients with amplification of the VEGFA genomic locus, the prevalence of this copy number aberration is low (5%–10%) (Horwitz et al., 2014; Llovet, 2014). Given the lack of effective treatment options for patients with advanced HCC, there is an urgent need to identify new druggable molecular targets.

EphA2 is a receptor tyrosine kinase implicated in many human diseases, including cancer, inflammatory disorders, and neurological disorders (Boyd et al., 2014; Kania and Klein, 2016; Pasquale, 2010). On binding with its ligands, ephrins, EphA2 activates its kinase activity, which leads to the autophosphorylation of its juxtamembrane Tyr residues (Y588 and Y594) (Binns et al., 2000; Fang et al., 2008). These events are essential for activation of ephrins-EphA2-directed cellular responses, including cell growth, migration, differentiation, and more (Kania and Klein, 2016; Pasquale, 2010). EphA2 overexpression can

This is an open access article under the CC BY-NC-ND license (http://creativecommons.org/licenses/by-nc-nd/4.0/).

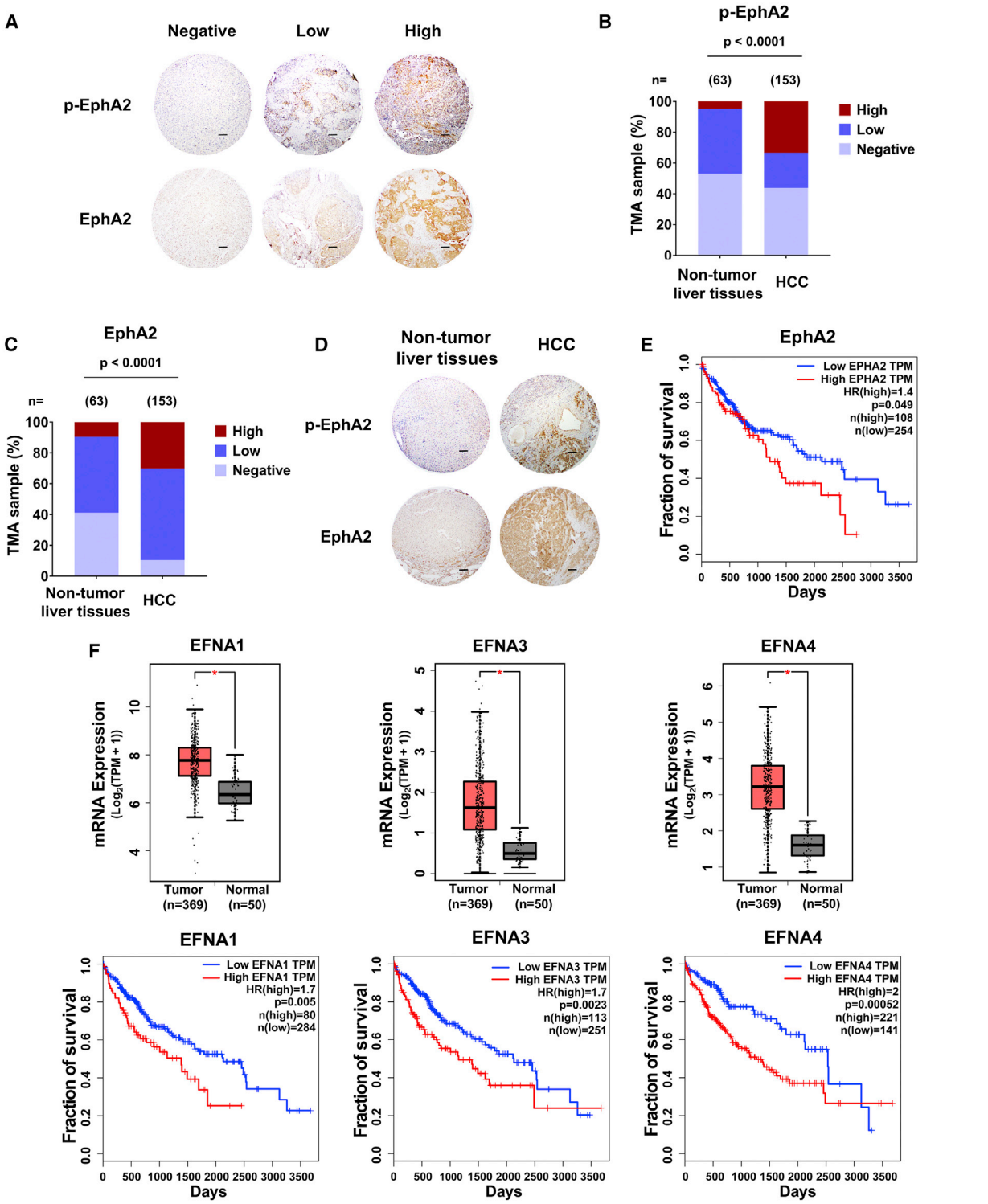

Figure 1. High EphA2 signaling and expression is detected in HCC patient samples and is associated with poor prognosis

(A) Representative IHC images of Y588 p-EphA2 and total EphA2 in HCC tissue microarray classified as negative, low, or high expression. Scale bars, 100 μm.

(B) Y588 p-EphA2 expression levels in TMAs of normal and HCC liver samples.

(C) Total EphA2 expression levels in TMAs of normal and HCC liver samples.

(D) Representative examples of normal versus HCC TMAs measured in (B) and (C). Scale bars, 100 μm.

(legend continued on next page)

also promote migration in glioma and prostate cancer cells in a ligand-independent manner (Miao et al., 2009).

Because EphA2 was initially discovered in human carcinomas over 30 years ago, many studies have investigated its functional roles in tumorigenesis (Hirai et al., 1987). High EphA2 expression and signaling are frequently detected in many cancers (including brain, breast, lung, etc.) and are associated with poor patient outcomes (Boyd et al., 2014; Pasquale, 2010; Wykosky and Debinski, 2008). For example, overexpression of EphA2 was sufficient to malignantly transform mammary epithelial cells (Hochgräfe et al., 2010; Zelinski et al., 2001). In glioblastoma, EphA2 promotes self-renewal and invasion of tumor-propagating cells (Binda et al., 2012; Miao et al., 2015). Recently, EphA2 expressed on tumor cells was shown to suppress T cell-mediated anti-tumor responses, and inhibition of EphA2 reversed T cell exhaustion and sensitized tumors to immunotherapy (Markosyan et al., 2019).

The role of EphA2 in HCC has not been well explored. Several clinical reports suggested that expression of EphA2 and its ligands correlated to tumor progression, invasion, metastasis, and poor prognosis in patients with HCC (Cui et al., 2010; Patil et al., 2009; Yang et al., 2009). Other studies have also shown that microRNAs impair tumorigenesis and enhance radiation therapy's efficacy through direct inhibition of EphA2 expression in HCC (Li et al., 2015; Xiang et al., 2019). Interestingly, a recent study showed that EphA2 is highly activated in sorafenib-resistant HCC cells, suggesting EphA2 may promote drug resistance to current therapy in HCC (Leung et al., 2020). However, the role of EphA2 and its mechanism of action in HCC development remain unknown. In this study, we discovered mechanisms underlying how EphA2 regulated tumor initiation and progression in HCC and explored the therapeutic potential of targeting EphA2 in HCC.

RESULTS

High EphA2 signaling and expression is detected in HCC patient samples and is associated with poor prognosis

Previous studies showed that phosphorylation at the juxtamembrane domain tyrosine 588 of EphA2 (Y588) is essential for its signaling activity (Binns et al., 2000; Fang et al., 2008). To explore the role of EphA2 signaling in HCC, we performed Y588 p-EphA2 and total EphA2 immunohistochemistry (IHC) on tissue microarrays from a retrospective cohort of 153 HCC specimens and 63 non-tumor liver tissues (Table S1). Y588 p-EphA2 and total EphA2 protein levels were assessed by a hepatic pathologist blinded to the patient outcome (Figures 1A and S1A). High expression of Y588 p-EphA2 and total EphA2 was detectable in 33.33% and 30.06% of HCC cases, respectively, while in non-tumor liver tissues, p-EphA2 and EphA2 high expression was only detectable in 4.76% and 9.52% of patients, respectively. Our results show that increased expression of p-EphA2 and total EphA2 correlates with HCC pathology (Figures 1B–1D). Furthermore, high mRNA expression of EphA2 in The Cancer Genome Atlas (TCGA) human HCC dataset was associated with poor prognosis (Figure 1E). Because Ephrin A class ligands (EFNAs) are known to activate EphA2 signaling (Boyd et al., 2014; Kania and Klein, 2016; Pasquale, 2010), we also analyzed the expression of EFNAs in the TCGA HCC dataset and found that 4 out of 5 EFNAs were highly expressed in HCC and were associated with poor prognosis (Figures 1F, S1B, and S1C). To further confirm these results, we analyzed another HCC cohort, GSE14520 (Roessler et al., 2010). In this cohort, although EphA2 expression (median cutoff) was not significantly associated with poor prognosis (Figure S1D), HCC patients with the highest (top 25%) expression of EphA2 had worse survival compared to the patients with lowest (bottom 25%) expression of EphA2 (Figure S1E). Among five ligands, high expression of EFNA4, but not others, was significantly associated with poor prognosis (Figures S1F–S1J). Hazard ratios analysis for 3-year survival also confirmed these findings (Table S2). The differences seen from these two cohorts might be due to different background, patient number, and other factors among the patients. Collectively, these data suggest that high EphA2 signaling is correlated with poor prognosis in HCC.

EphA2 drives HCC tumor growth

In light of these observations, we sought to test the functional role of EphA2 signaling in HCC. First, we assessed EphA2 expression and activity in seven human HCC cell lines and found all expressed EphA2 and Y588 p-EphA2 (Figure 2A). Next, we selected three human HCC cell lines with high or modest levels of p-EphA2 and EphA2 expression (Huh7, Hep3B, and SNU475) and attenuated the expression of EphA2 by lentiviral-short hairpin RNA (shRNA) knockdown (Figure 2B). We found that knockdown of *EphA2* impaired the proliferation of all these HCC cells (Figure 2C). To verify the role of EphA2 in HCC *in vivo*, we established xenograft models with Huh7 cells (control or shRNA-mediated suppression of *EphA2*). Following implantation of tumor cells at day 0, controls showed the first sign of tumor at ~18 days and a linear increase in tumor volume during the subsequent week. In contrast, *EphA2* knockdown mice showed no tumor sign for up to 28 days (Figure 2D). We observed similar results in the Hep3B xenograft models (Figure 2E). All cells for xenograft studies were screened for viability via Trypan blue before injection; however, we cannot rule out a possible role of EphA2 in maintenance/survival after cell implantation. Overall, our results suggested that EphA2 is crucial for tumor growth in HCC.

Targeting EphA2 suppresses tumor initiation and progression and enhances overall survival in MET/CAT induced murine model of HCC

We have previously utilized several established genetically engineered mouse models (GEMM) of HCC to study hepatocarcinogenesis (Shang et al., 2015, 2019; Wang et al., 2018). The advantages of the GEMM model are: (1) tumor develops at its site of

(E) Kaplan-Meier plot of overall survival of HCC patients stratified by EphA2 expression levels from the TCGA database (GEPIA).
(F) Top: a boxplot of relative mRNA expression levels of EFNAs comparing normal versus HCC tissue. Bottom: Kaplan-Meier plot of overall survival of HCC patients stratified by EFNA expression levels. Data from TCGA (GEPIA).
Statistical significance was determined by chi-square test (B) and (C), two-tailed Student's t test *$p < 0.0001$ boxplots (F), and log-rank test Kaplan-Meier plot (E and F).

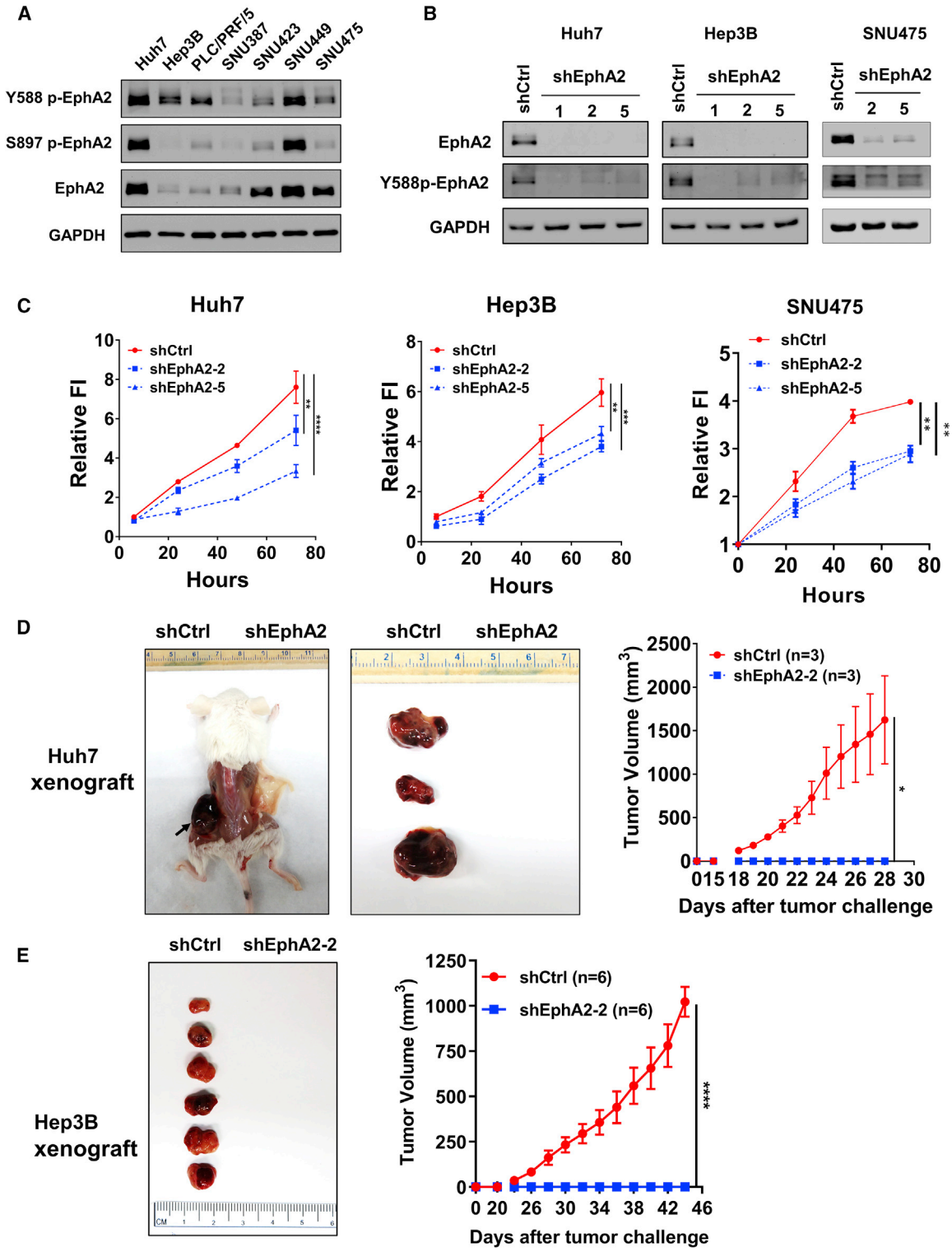

Figure 2. EphA2 drives HCC tumor proliferation and initiation

(A) Western blot showed EphA2 activation in 7 independent HCC cell lines. GAPDH as a loading control.

(B) Western blot validated *EphA2* knockdown efficiency after lentiviral transduction of 3 independent *EphA2* shRNAs 7 days after puromycin selection.

(legend continued on next page)

origin and retains its native vasculature and microenvironment; (2) mice are immunocompetent; and (3) mice exhibit comparable clinical symptoms such as hepatomegaly and ascites. To further determine the role of EphA2 in HCC development, we used the c-MET (MET)/β-catenin (CAT)-driven HCC model, which is useful for studying the functions of genes in HCC development because of its clinical relevance (Cieply et al., 2009; Kaposi-Novak et al., 2006; Tao et al., 2016; Tward et al., 2007). Both p-EphA2 and EphA2 are highly expressed in MET/CAT-induced liver tumors (Figure 3A). To study the role of EphA2 in this model, we combined the MET/CAT model with CRISPR-Cas9-mediated inhibition of EphA2 expression in the mouse liver (Figure 3B) (Cong et al., 2013; Xue et al., 2014). We cloned three pX330 vectors, each co-expressing Cas9 and 1 of 3 independent single guide RNAs (sgRNAs) selected to target *EphA2*. Of the three sgEphA2 constructs tested, sgEphA2-2, was chosen for further experiments because of its high knockout efficacy (Figure 3C). The effectiveness and specificity of sgEphA2-2 were further validated using immunofluorescence and immunoblot (Figures 3D and 3E). Ten days after the injection of MET/CAT, almost all of the transformed hepatocytes, which expressed high c-MET, also had high EphA2 expression (Figure 3E), while there was very little detectable EphA2 in normal murine liver tissue or non-transformed cells (Figures 3A and 3E). These data suggest that detectable EphA2 was specifically induced in transformed cells. Because hydrodynamic injection equivalently delivers plasmids into the same cells (Sebestyén et al., 2006; Shang et al., 2015), sgEphA2-2 efficiently deleted EphA2 in the transformed cells, which was indicated by almost complete ablation of the EphA2 signals in mouse liver (Figure 3E).

Notably, mice receiving sgEphA2-2 had a significant reduction of tumor burden compared to the control on day 45 after the injection, whereas the control mice developed ascites, hepatomegaly, and tumor mass (Figures 3F, 3G, and S2A). Histologic examination of PX330 control livers showed hallmark HCC features, including increased cellular density, nuclear polymorphism, vesicular chromatin, intratumor, and extramedullary hematopoiesis with nucleated red blood cells (Figure 3H). Immunohistochemical staining for alpha-fetoprotein (AFP), an HCC marker, was dramatically lower in the livers of sgEphA2-2 mice compared to PX330 control mice (Figure 3H). Significantly, all of the PX330 control mice died with advanced liver cancer within 37–65 days, whereas sgEphA2-2 mice developed tumors at long latency, as 45% of the mice were symptom-free and were still alive beyond 106 days (Figure 3I). Intriguingly, sgEphA2-2 mice that eventually developed HCC had re-expression of EphA2 in the tumor region (Figures S2B and S2C). These data suggest that deletion of EphA2 was incomplete, resulting in eventual initiation and development of long-latency tumors in these mice. Taken together, our results demonstrate that EphA2 is an important promotor for the initiation and development of MET/CAT induced HCC.

EphA2 promotes the development of HCC partially through activation of the AKT pathway

To investigate the underlying mechanism of EphA2-induced tumor development, we performed RNA sequencing on *EphA2* knockdown and scrambled control Huh7 cells. Gene set enrichment analysis (GSEA) revealed that many signaling pathways (Table S3A), including genes induced by AKT signaling (Figure 4A), were affected by EphA2 knockdown. AKT signaling drew our attention because AKT has been shown to play a critical role in promoting HCC development (Galicia et al., 2010; Grabinski et al., 2012; Stauffer et al., 2011). Previous studies have also demonstrated that the modality of EphA2 regulation of AKT is highly variable and tissue-dependent; that is, ligand-induced EphA2 signaling can either activate or inhibit AKT under different conditions (Chang et al., 2008; Miao et al., 2009; Pasquale, 2010). In line with our RNA-sequencing data, we found that phosphorylation of AKT at both Ser473 and Thr308 sites, which are critical for AKT activation (Alessi et al., 1996; Song et al., 2019), was substantially suppressed in both Huh7 and Hep3B *EphA2* knockdown cells compared with the scrambled control (Figure 4B). Similarly, knocking out *EphA2* decreased AKT activity in our MET/CAT model of HCC (Figures S3A–S3D). Overexpression of EphA2 increased AKT activation in PLC/PRF/5 cells (Figure S3E), which expresses a low level of EphA2 (Figure 2A). Overall, these data suggest that EphA2 promotes AKT signaling in the context of HCC.

To further validate our hypothesis regarding the relationship between EphA2 and AKT in HCC, we expressed a constitutively active form of AKT (CA-AKT) in the context of *EphA2* knockdown Huh7 cells (Figure 4C). Expression of CA-AKT rescued the proliferation of EphA2 knockdown cells *in vitro* (Figure 4D). Intriguingly, when tumor cells were implanted in our HCC xenograft model, CA-AKT expression only partially rescued tumor growth in *EphA2* knockdown cells (Figure 4E). Moreover, MK-2206, a selective inhibitor of pan-AKT, suppressed AKT activity, and HCC cell growth (Figures S4A–S4C). Overall, the results suggest that EphA2 drives the development of HCC partially through AKT signaling.

EphA2 drives HCC tumor development partially through activation of STAT3 signaling

Because expression of CA-AKT only partially rescued tumor development in *EphA2* knockdown cells in xenograft models, we suspected that additional signaling pathways might be

(C) Cell proliferation studies of control versus EphA2 knockdown Huh7, Hep3B, and SNU475 cells at day 7 after puromycin selection. Cell proliferation was evaluated using the Alamar blue assay. The ratio of proliferation is normalized to at 6 h after initial seeding of the cells and measured at 24, 48, and 72 h. Values are mean ± SD (n = 4).

(D) Left: representative picture of NSG-A2 mice 28 days after injection with 3×10^6 Huh7 cells. Left flank: shCtrl. Right flank: shEphA2. N = 3 mice per group. Right, daily measurements of primary tumor size. Values are mean ± SEM.

(E) Left: representative picture of NSG-A2 mice 44 days after injection with 3×10^6 Hep3B cells. Left flank: shCtrl. Right flank: shEphA2. N = 6 mice per group. Right, daily measurements of primary tumor size. Values are mean ± SEM.

Statistical significance was determined by one-ANOVA analysis with Dunnett's multiple comparisons test (C) or two-tailed Student's t test (D and E); *$p < 0.05$, **$p < 0.01$, ***$p < 0.001$ and ****$p < 0.0001$.

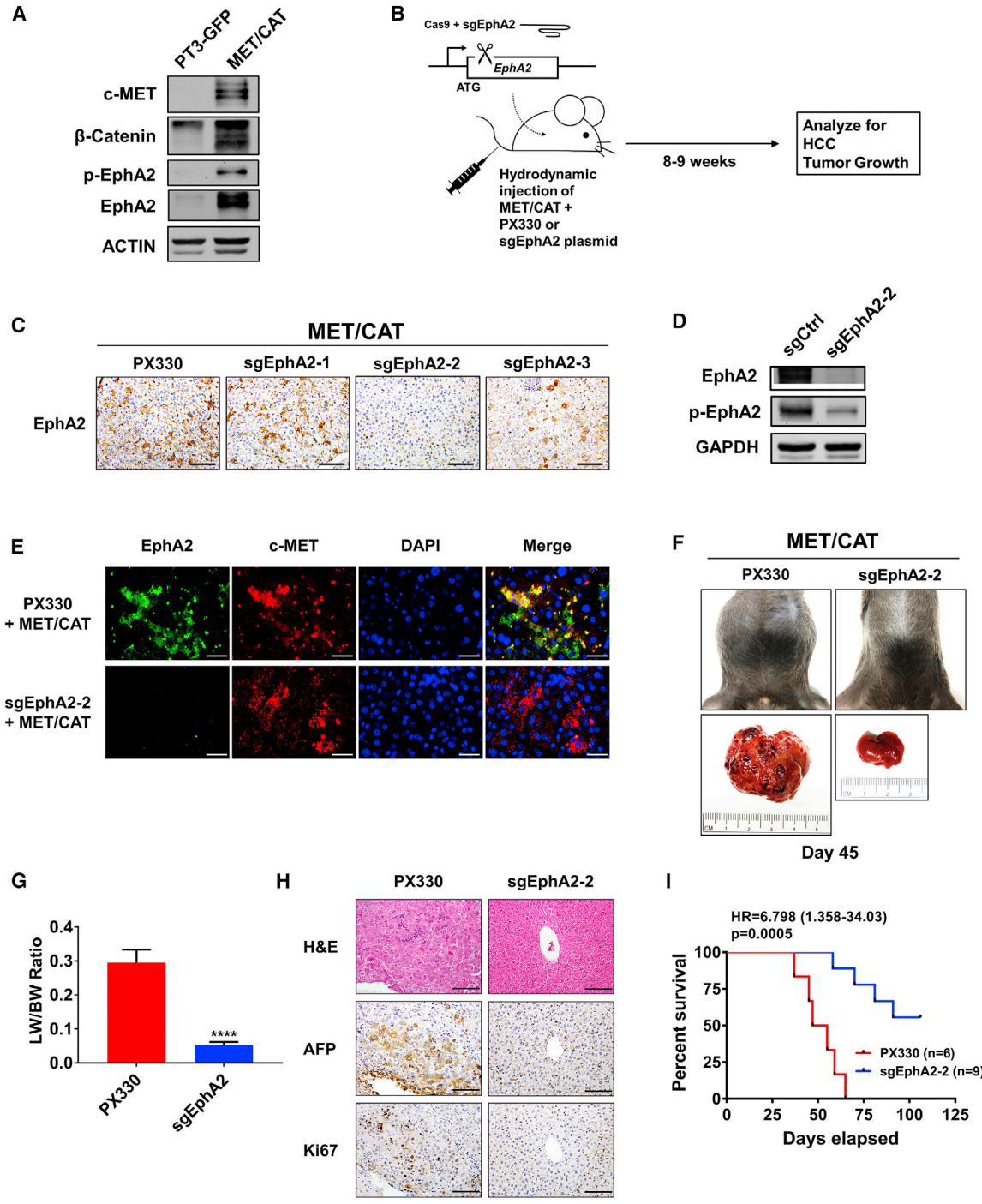

Figure 3. Targeting EphA2 suppresses tumor progression and enhances overall survival in MET/CAT-induced murine model of HCC

(A) Western blot validating MET/CAT HCC model and analyzing for EphA2 signaling and expression. ACTIN as a loading control.

(B) Schematic of the experiment of targeted inhibition of EphA2 in MET/CAT induced murine HCC model. pX330 plasmids expressing Cas9 and sgRNA targeting EphA2 (sgEphA2) or empty vector (PX330) were hydrodynamically delivered to mice liver in conjunction with MET/CAT; mice were observed for development of HCC for 8–9 weeks. n = 6 mice in the PX330 group, and n = 9 mice in the sgEphA2 group.

(C) IHC validated the efficacy of 3 independent sgEphA2 constructs in MET/CAT model 10 days after injection. Scale bars, 100 μm.

(D) Western blot confirmed the efficacy of sgEphA2-2 in MET/CAT model 10 days after injection. GAPDH as a loading control.

(E) Immunofluorescence analyzing *EphA2* knockout in the context of MET overexpression in MET/CAT model 10 days after injection. EphA2, green;, c-MET, red. Nuclei were stained with DAPI (blue). Scale bars, 30 μm.

(legend continued on next page)

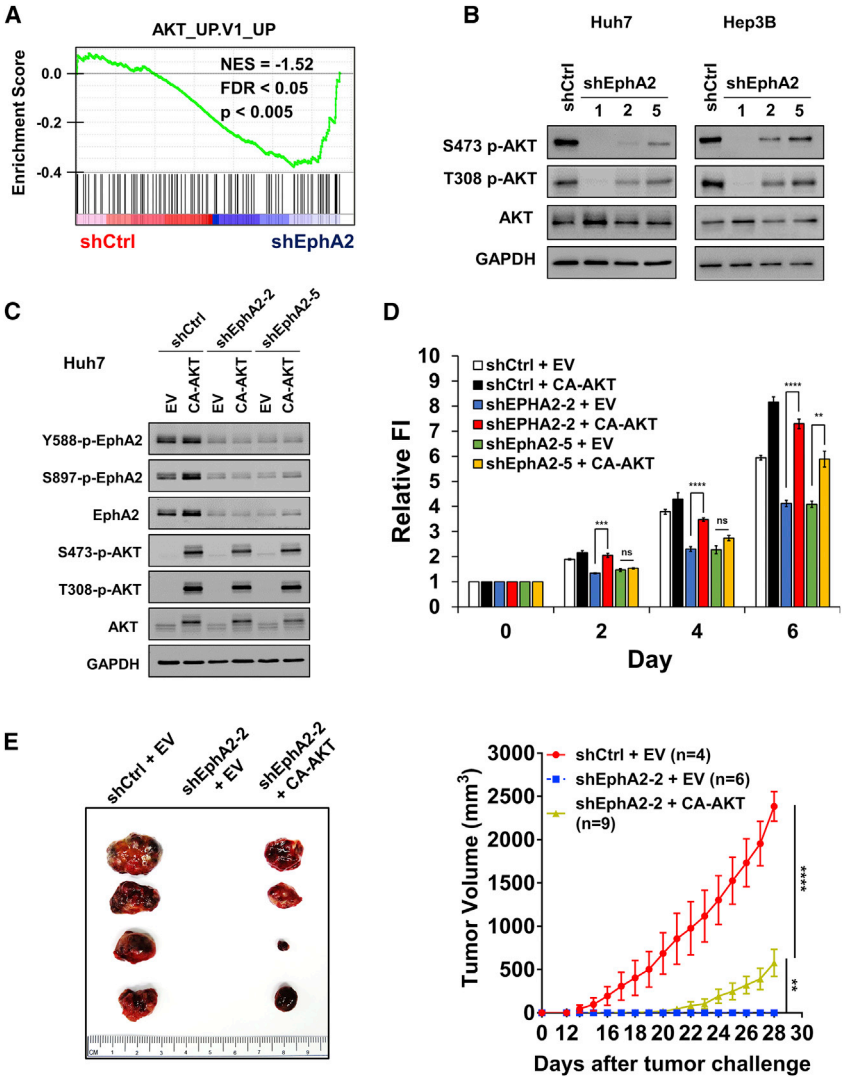

Figure 4. EphA2 promotes the initiation and growth of HCC partially through activation of the AKT pathway

(A) GSEA revealed that genes in the AKT pathway are highly enriched in *EphA2* knockdown Huh7 cells.

(B) Cell lysate of EphA2 knockdown Huh7 and Hep3B cells were immunoblotted for p-AKT and total AKT. GAPDH as a loading control.

(C) Western blot validated overexpression of constitutively active AKT (CA-AKT) in the context of two independent shRNA mediated *EphA2* knockdown in Huh7 cells.

(D) Cell proliferation study was conducted using cells described in (C) using the Alamar blue assay. Fluorescence intensity was measured at day 0 (6 h after seeding) and subsequently at day 2, 4, and 6. Values are mean ± SD (n = 4).

(E) Left: representative picture of tumors extracted from NSG-A2 mice 28 days after subcutaneous injection with cells described in (C) and (D). n = 4, 6, 9 mice in shCtrl + EV, shEphA2 + EV, and shEphA2 + CA-AKT, respectively. Right: daily measurements of primary tumor size. Values are mean ± SEM.

Statistical significance was determined by two-tailed Student's t test (D) and one-ANOVA analysis with Dunnett's multiple comparisons test (E) **p < 0.01, ***p < 0.001 and ****p < 0.0001.

involved in EphA2 signaling. RNA-sequencing data indicated that the JAK/STAT3 pathway is the second most enriched pathway affected by *EphA2* knockdown (Figure 5A; Table S3A), suggesting that STAT3 is a downstream target of EphA2 in HCC. STAT3 is a crucial oncogene that promotes tumor initiation and progression in a majority of human malignancies, including HCC (Calvisi et al., 2006; He and Karin, 2011; He et al., 2010a; Huynh et al., 2019; Johnson et al., 2018; Li et al., 2006; Yu et al., 2014). In addition, STAT3 signaling promotes stem-cell-like properties in cancers by transcription of crucial pluripotent factors such as SOX2 and KLF4, leading to tumor initiation, relapse, and drug resistance (Hall et al., 2009; Huynh et al., 2019; Schroeder et al., 2014; Yu et al., 2014). A previous study showed that EphA2 acts against fungal infection by increasing JAK2/STAT3 signaling (Swidergall et al., 2018); however, no study has reported EphA2 signaling can activate STAT3 in cancer. Although knockdown of EphA2 did not affect STAT3 mRNA expression levels in HCC cells (Figure S5A), EphA2 knockdown in HCC cells suppressed phosphorylation of STAT3 at Tyr705 (Figure 5B), which is critical for STAT3 activation (Darnell et al., 1994). Notably, the level of total STAT3 was also decreased by knockdown of EphA2 in HCC cells (Figure 5B), which might be due to reduced phosphorylation of STAT3, because several studies showed that tyrosine phosphorylation, such as at the Y705 position, stabilizes STAT3 protein (Murase, 2013; Park et al., 2000). Similarly, knocking out *EphA2* attenuated STAT3 activity in our MET/CAT HCC model (Figures 5C, S3A, S3C, S3D, and S6A). Additionally, overexpression of EphA2 increased

(F) Top: a representative image of the mouse abdomen in MET/CAT mouse treated with PX330 or sgEphA2 45 days after injection. Bottom: gross pictures of livers extracted from mice from the upper panels.

(G) Liver-to-bodyweight ratios were calculated for MET/CAT mice injected with PX330 or sgEphA2 for 8 weeks (56 days). N = 3 mice per group.

(H) Livers of MET/CAT mice injected with PX330 or sgEphA2 were collected at day 45 for H&E and IHC for HCC and proliferative markers, AFP and Ki67. Scale bars, 100 μm.

(I) Kaplan-Meier plot for experiment illustrated in (B) represented the percent of survival (y axis) at days elapsed after injection (x axis).

Statistical significance was determined by the two-tailed Student's t test ****p < 0.0001 (G) and log-rank test (I).

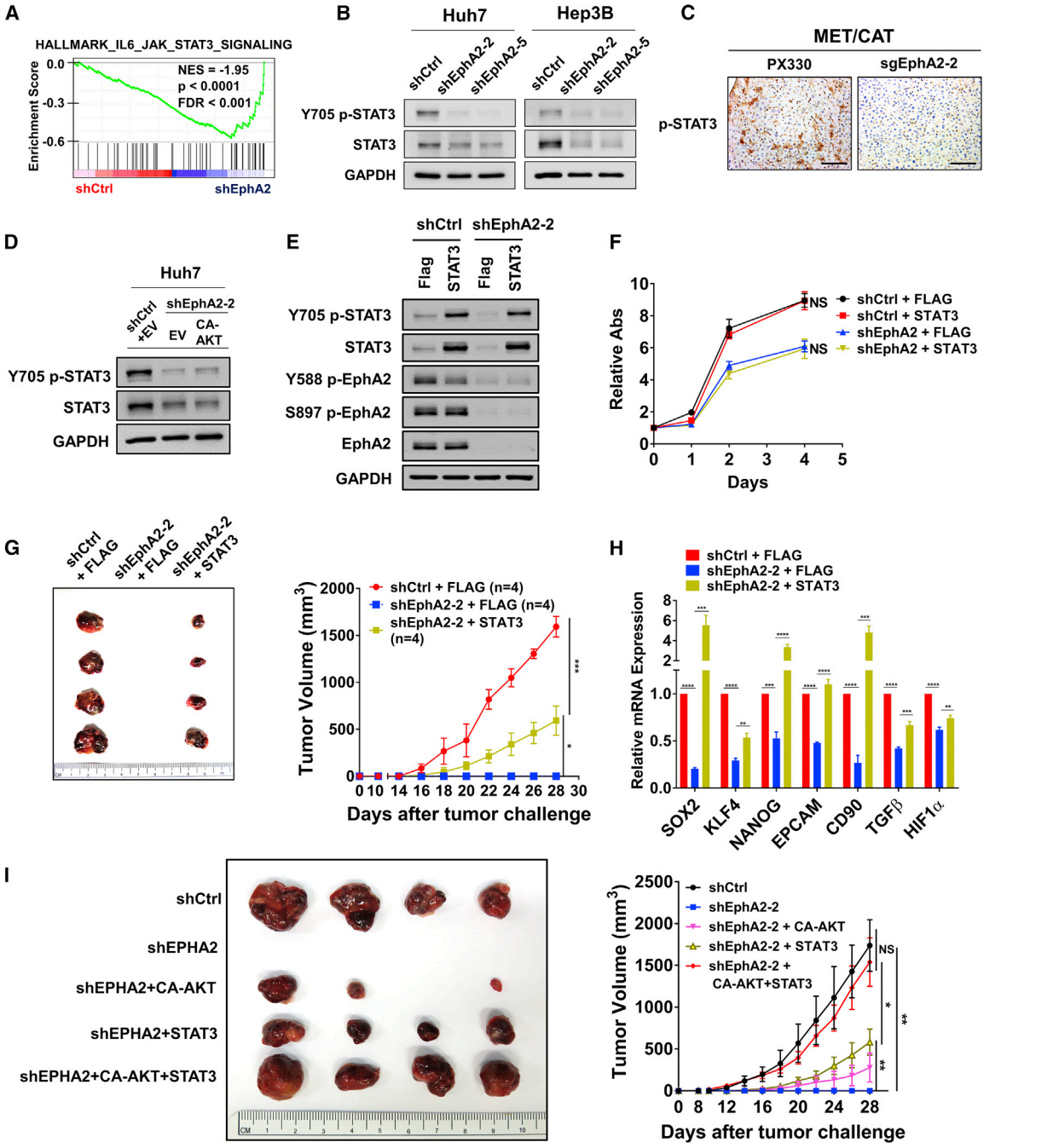

Figure 5. EphA2 drives tumor initiation and development partially through activation of STAT3 signaling

(A) GSEA revealed that genes in the JAK/STAT3 pathway are highly enriched in *EphA2* knockdown Huh7 cells.

(B) Cell lysate of EphA2 knockdown Huh7 and Hep3B cells were immunoblotted for p-STAT3 and total STAT3. GAPDH as a loading control.

(C) Liver of *EphA2* knockout MET/CAT mice was extracted and immunohistochemically assessed for p-STAT3 expression comparing to control (PX330). Scale bar, 100 μm.

(D) Cell lysate of *EphA2* knockdown Huh7 cells with overexpression of CA-AKT was immunoblotted for p-STAT3 and total STAT3.

(E) Western blot validated overexpression of STAT3 in the context of shRNA mediated *EphA2* knockdown in Huh7 cells.

(F) Cell proliferation study was conducted using cells described in (C) using the Alamar blue assay. The ratio of proliferation was calculated by normalizing fluorescent intensity to day 0 (6 h after seeding of the cells) and subsequently measured at day 1, 2, and 4 days. Values are mean ± SD (n = 4).

(G) Left: representative picture of tumors extracted from NSG-A2 mice 28 days after subcutaneous injection with cells described in (E) and (F). n = 4 mice in each group. Right: primary tumor size was recorded every 2 days. Values are mean ± SEM.

(H) qPCR analysis of the indicated gene expression in HCC cells described in (F). Values are mean ± SD (n = 3).

(legend continued on next page)

STAT3 signaling in PLC/PRF/5 cells (Figure S3E). These results provide evidence that STAT3 is a downstream effector of EphA2 signaling in HCC. Previous studies showed that STAT3 could be a downstream effector of AKT signaling (Abdelhamed et al., 2016; Yokogami et al., 2000). We found that overexpression of CA-AKT did not affect STAT3 signaling in shEphA2 cells (Figure 5D). Consistently, inhibition of AKT by MK-2206 did not suppress STAT3 activity in parental HCC cells (Figures S4A and S4B). These results suggest that regulation of STAT3 by EphA2 in HCC is not through AKT signaling.

Further, we found that STAT3 overexpression had no significant effect on the growth of scrambled Huh7 cells *in vitro* and *in vivo* (Figures 5E, 5F, S6B, and S6C). STAT3 overexpression also did not affect the proliferation of *EphA2* knockdown Huh7 cells *in vitro* (Figure 5F). However, BBI608, a STAT3 inhibitor, suppressed STAT3 activity, and HCC cell growth in Huh7 cells without affecting AKT activity (Figures S6D and S6E). The results suggest that overexpression of STAT3 alone is not sufficient to promote HCC cell growth, but STAT3 activity is necessary for HCC cell growth. In the Huh7 xenograft model, overexpression of STAT3 significantly rescued and initiated tumor growth in the *EphA2* knockdown condition (Figure 5G), and a repertoire of tumor-initiating and pluripotent factors suppressed in the *EphA2* knockdown was dramatically rescued by STAT3 overexpression in HCC cells *in vitro* (Figure 5H). Overall, these results show that EphA2 drives tumor development also partially through activating STAT3. Furthermore, the combined overexpression of CA-AKT and STAT3 almost completely rescued the reduced tumor development by EphA2 knockdown in a xenograft model (Figures 5I and S6F), and demonstrates that EphA2 drives tumor development mainly through the activation of both AKT and STAT3 signaling.

EphA2 activates STAT3 signaling via JAK1 in HCC

Next, we investigated how EphA2 activates STAT3 in HCC. JAK family non-receptor tyrosine kinases (JAKs) can directly activate STAT3 through canonical activation of STAT3 in many malignancies, including HCC (Johnson et al., 2018; Yu et al., 2014). JAKs can be activated by RTKs such as EGFR, PDGFR, and FGFR (Andl et al., 2004; Huynh et al., 2019), which led us to test whether EphA2 activates STAT3 via JAKs. RNA-sequencing data showed that JAK1 had substantial expression in HCC cells while the expression of JAK2 was modest, and JAK3 expression was very low (Figure S7A). We further confirmed that little JAK2 protein expression was detected in HCC cells by immunoblot (Figure S7B). We, therefore, examined if EphA2 can activate JAK1 in HCC cells. Phosphorylation of JAK1 at Tyr1034/1035, which is critical for activation of JAK1 (Leonard and O'Shea, 1998), was suppressed when EphA2 was knocked down in both Huh7 and Hep3B cells (Figure 6A). Suppression of JAK1 phosphorylation was associated with substantially lower STAT3 activation (Figure 6A). Knocking out *EphA2* in the MET/CAT model of HCC also suppressed JAK1 activation (Figures 6B, S3A, S3C, and S3D). Furthermore, we knocked down JAK1 in both Huh7 and Hep3B using small interfering RNA (siRNA) and found that STAT3 signaling was attenuated by JAK1 knockdown (Figure 6C). Moreover, treatment with a JAK inhibitor (pyridine 6) (Thompson et al., 2002) potently inhibited STAT3 signaling in Huh7 cells (Figure S7C).

Interleukin (IL)-6 can activate JAK1/STAT3 and plays a critical role in HCC development (Bergmann et al., 2017; Lokau et al., 2019). We found no significant decrease in transcript levels of IL-6/GP130 family genes except IL-6ST (a modest reduction) in EphA2 knockdown Huh7 cells compared to scramble control (Figure S5B). We further performed western blot and found the protein levels of GP130 were not significantly changed by EphA2 knockdown (Figure S5C). Besides, secreted IL-6 levels were comparable in cell culture supernatants of EphA2 knockdown and scrambled HCC cells (Figure S5D). These data suggest that the mechanism of EphA2 in promoting STAT3 activity is most likely not due to paracrine or autocrine regulation of IL-6. A previous study showed that EphA4, another member of the Ephrin receptor family, can directly interact with JAK2 and activate STAT3 signaling at the neuromuscular junction (Lai et al., 2004), raising the possibility that EphA2 can activate STAT3 in a similar manner. Notably, using proximity ligation assay (PLA) (Söderberg et al., 2006; Weibrecht et al., 2010), we found notable interaction between EphA2 and JAK1 in the scrambled HCC cells, which was significantly reduced by the *EphA2* knockdown (Figure 6D). Taken together, these results indicate that EphA2 promotes STAT3 signaling through activation of JAK1.

EphA2 signaling is positively correlated with AKT and JAK1/STAT3 activation in HCC patient samples

Our data show that EphA2 promotes HCC initiation and development by activating both AKT and JAK1/STAT3 in cell-based and animal models. To determine whether the EphA2/AKT and EphA2/JAK1/STAT3 axes are relevant in human HCC, we examined p-EphA2, p-AKT, p-JAK1, and p-STAT3 by IHC in a tissue microarray including 153 human HCC specimens. Notably, p-EphA2 expression was positively correlated with the activation status of AKT, JAK1, and STAT3 within the same tumor region (Figures 6E–6I). There was also a strong positive correlation between p-JAK1 and p-STAT3 expression, highlighting the importance of JAK1 as an activator of STAT3 in HCC (Figure 6J). Taken together, these results suggest that EphA2 activates both AKT and JAK1/STAT3 signaling in human HCC.

Pharmacologic targeting of EphA2 impairs growth and progression of HCC *in vitro* and *in vivo*

So far, we have shown that the receptor tyrosine kinase-EphA2-is a critical oncodriver that promotes the initiation and progression of HCC. Given the success of targeting RTKs with specific small molecule kinase inhibitors (Ferguson and Gray, 2018), we next explored the translational potential of targeting EphA2

(I) Left: representative picture of tumors extracted from NSG-A2 mice 28 days after subcutaneous injection with the indicated cells. n = 4 mice in each group. Right: primary tumor size was recorded every 2 days. Values are mean ± SEM.

Statistical significance was determined by one-ANOVA analysis with Tukey's multiple comparisons test (F) and (G) and two-tailed Student's t test (H). NS, not significant; *p < 0.05, **p < 0.01, ***p < 0.001 and ****p < 0.0001.

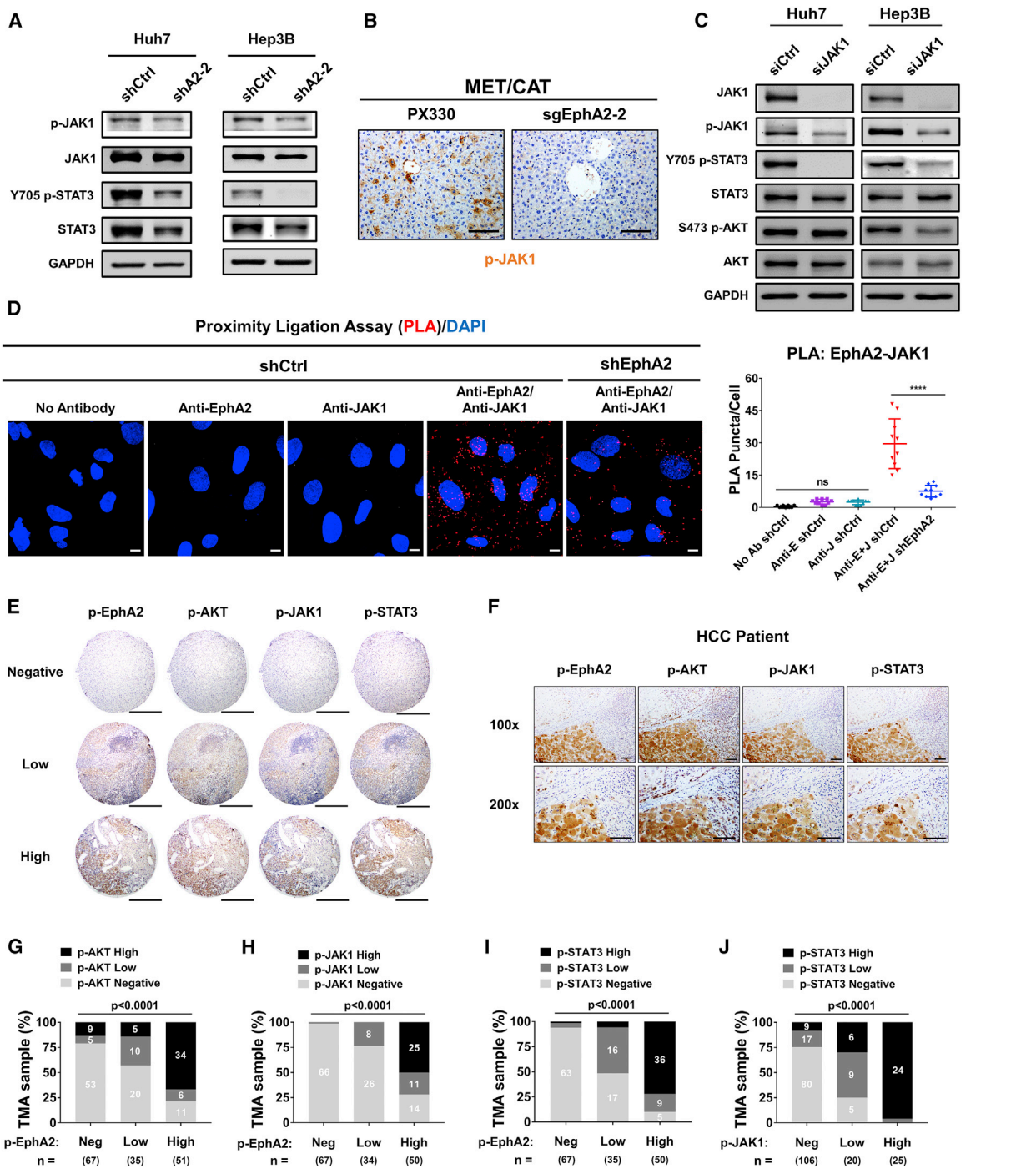

Figure 6. EphA2 activates STAT3 signaling via JAK1 in HCC, and EphA2 signaling is positively correlated with AKT and JAK1/STAT3 activation in HCC patient samples

(A) Cell lysate of EphA2 knockdown Huh7 and Hep3B cells were immunoblotted for p-JAK1, JAK1, p-STAT3, and total STAT3. GAPDH as a loading control.

(B) The liver of EphA2 knockout MET/CAT mice was extracted, and IHC was used to assess for p-JAK1 expression comparing to control (PX330). Scale bar, 100 μm.

(C) Huh7 and Hep3B cells were transfected with siRNA targeting JAK1. 48 h after the transfection, the protein was extracted and immunoblotted for JAK1, p-JAK1, p-STAT3, STAT3, p-AKT, and AKT expression.

(D) Left: the interaction of EphA2 and JAK1 was quantified using proximity ligation assay (PLA) in Huh7 scramble (shCtrl) and EphA2 knockdown (shEphA2) cells. Positive PLA interaction (red). Nuclei were stained with DAPI (blue). Scale bar, 10 μm. Right: PLA Puncta per cell was quantified using Imaris Bitplane, n = 10. Statistical significance was determined by one-ANOVA analysis with Tukey's multiple comparisons test (D). ns, not significant; *p < 0.05, ****p < 0.0001.

(legend continued on next page)

with the small molecule inhibitor ALW-II-41-27 (ALW). ALW is a potent and selective EphA2 inhibitor, which was recently shown to exhibit anti-tumor activity in many solid malignancies (Amato et al., 2014, 2016; Choi et al., 2009; Martini et al., 2019). ALW potently impaired the growth of all six HCC cell lines (Figure 7A). In addition, ALW effectively decreased the phosphorylation of EphA2 at Y588 and its downstream effectors (p-AKT, p-JAK1, and p-STAT3) in HCC cells (Figure 7B). To test the effect of ALW on HCC *in vivo*, we treated mice from a human xenograft model of HCC with ALW and observed the impact on tumor growth. We found that while the vehicle-treated control tumors grew rapidly, the ALW-treated tumors showed complete inhibition of tumor growth for 7 days and notably even showed tumor regression for the first 3 days of treatment (Figure 7C). Furthermore, consistent with *in vitro* data, tumors of mice treated with ALW showed a dramatic decrease in phosphorylation of EphA2 and its downstream targets p-AKT, p-JAK1, and p-STAT3 (Figure 7D). Overall, these results demonstrated that therapeutic targeting of EphA2 impaired the growth and progression of HCC *in vitro* and *in vivo*.

DISCUSSION

HCC remains one of the most lethal malignancies worldwide because of the immense challenges in preventing, diagnosing, and treating the disease (Villanueva, 2019). The currently approved medications for advanced HCC provide patients with limited clinical benefits (Llovet et al., 2015; Villanueva, 2019). A significant barrier to drug development is the lack of understanding of critical drivers of oncogenesis and tumor progression (Llovet et al., 2015). Here, we established EphA2 as an oncogene that promotes tumor initiation and progression in HCC, and inhibition of EphA2 suppressed HCC tumor initiation and growth. We found that high EphA2 signaling and expression is observed in over 33% of HCC patient samples and is associated with worse clinical outcomes. Therefore, many HCC patients may benefit from the inhibition of EphA2 signaling.

The nature of EphA2 signaling is highly diverse and tissue-dependent, and many studies have reported contradictory responses from the same ligand-EphA2 interaction in different cell types (Pasquale, 2010; Wykosky and Debinski, 2008). The reasons for this are still unclear. One possible explanation is that spatial-mechanical properties of EphA2 clustering elicit different downstream signaling based on the chemo-physical properties of the inherent cell type (Himanen et al., 2010; Kania and Klein, 2016; Salaita et al., 2010). Furthermore, tissue-specific responses are driven by the pre-programmed epigenetic signatures across tissue types (Haigis et al., 2019). Thus, differential clustering of EphA2 governed by pre-determined epigenetic landscape allows for a wide array and even contradictory cellular responses across cancers, highlighted by how EphA2 regulates AKT in different cancers. For example, in glioblastoma, ligand-induced EphA2 signaling inactivates AKT by dephosphorylation (Miao et al., 2009). In contrast, the same ligand-induced EphA2 signaling promotes AKT signaling by phosphorylation in pancreatic cancer (Chang et al., 2008). We found that functional inhibition of EphA2 decreases AKT activity in HCC cells, suggesting that EphA2 activates AKT in HCC, further supported by the evidence that EFNA1-Fc (a soluble recombinant EphA2 ligand) activated AKT signaling in HCC cells (Figure S7D). AKT is activated in up to 31.2% of HCC cases and plays a crucial role in the malignant transformation of hepatocytes to HCC (Matter et al., 2014; Villanueva et al., 2008). EphA2 activation is significantly associated with high levels of AKT activity in human HCC (Figure 6G). Therefore, targeting EphA2 could provide an effective therapeutic strategy for AKT-driven HCC. It is notable that shEphA2-2 HCC cell clones expressed less activated AKT (Figure 4B), but proliferated faster than the shEphA2-5 cell clones (Figure 2C). One explanation is that EphA2-mediated HCC cell proliferation is not solely dependent on AKT signaling, and there are other mechanisms involved. It is also possible that alterative or compensatory pathways are activated when knockdown of EphA2 suppresses AKT signaling. We will look into these possibilities in our future studies.

STAT3 is a crucial oncogene in many cancers, including HCC (He and Karin, 2011; Yu et al., 2014). Targeting STAT3 could provide numerous benefits, including inhibition of tumor initiation, growth, metastasis, and resistance to conventional therapy and immunotherapy (Huynh et al., 2019; Johnson et al., 2018; Yu et al., 2014). However, STAT3 is often deemed "undruggable" due to the lack of an intrinsic enzymatic site (Wong et al., 2017). Here, we discovered that EphA2 activates STAT3 in HCC, which is further supported by the finding that EFNA1-Fc activated STAT3 in HCC cells (Figure S7D). We found that STAT3 activation by EphA2 in HCC is not through AKT or para-/autocrine regulation of IL-6. Instead, we demonstrated that EphA2 promoted STAT3 through the regulation of JAK1 in HCC cells. Further, we observed a direct interaction between EphA2 and JAK1 in HCC cells. Intriguingly, we found that JAK1 and EphA2 interact in the perinuclear region (Figure 7D), despite JAKs being canonically thought to be exclusively in the cytoplasm associated with transmembrane receptor proteins on the cell membrane (Darnell et al., 1994; Stark et al., 1998). Although the exact mechanism is unclear, EphA2 may exhibit perinuclear endosomal signaling to activate JAK1/STAT3. Many studies have shown that RTKs, on ligand binding and activation, are internalized and can continue to recruit and activate signaling pathways within intracellular vesicles (Kermorgant and Parker, 2008; Sigismund et al., 2008). Furthermore, studies have shown that EphA2 exhibits diverse signaling in endosomes, especially in the perinuclear region (Boissier et al., 2013; Sabet et al., 2015). Reports also demonstrated that EGFR requires

(E) Representative immunohistochemistry (IHC) images and correlation of Y588 p-EphA2, p-AKT, p-JAK1, and p-STAT3 in HCC tissue microarray classified as negative, low, or high expression. Scale bars, 500 μm.

(F) Representative high-power magnification of IHC images of HCC showing a correlation between Y588 p-EphA2, p-AKT, p-JAK1, and p-STAT3. Scale bar, 100 μm.

(G–J) Correlation analysis of all HCC TMA tissues between Y588 p-EphA2 and p-AKT (C), p-EphA2 and p-JAK1 (D), Y588 p-EphA2 and p-STAT3 (E), and p-JAK1 and p-STAT3. Statistical significance was determined by a chi-square test (C–F).

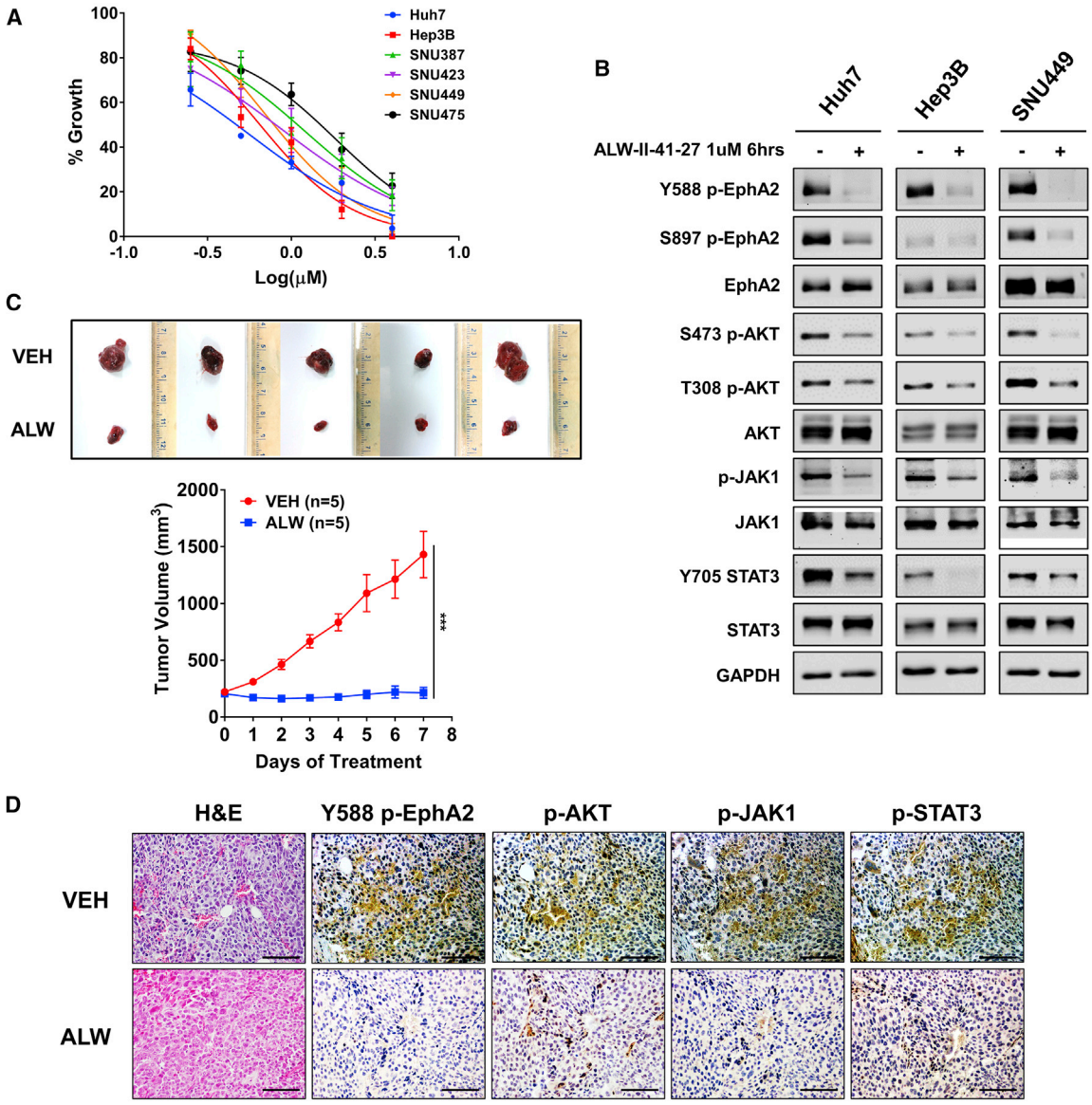

Figure 7. Pharmacologic targeting of EphA2 impairs growth and progression of HCC *in vitro* and *in vivo*

(A) The effect of ALW-II-41-27 on cell proliferation of 6 HCC cell lines was assessed after 48 h of treatment using Alamar blue assay. Data are shown as percent of fluorescence comparing to DMSO control. Values are mean ± SD (n = 4).

(B) Western blot analysis of indicated proteins at the selected time and concentration of ALW-II-41-27 in Huh7, Hep3B, and SNU449 cells. GAPDH as a loading control.

(C) Image of tumors extracted from NSG-A2 mice subcutaneously injected with 5 × 10^6 Huh7 cells; 7 days after treatment with 15 mg/kg/day ALW-II-41-27 or vehicle. Treatment began after the tumor reached 200 mm^3. n = 5 mice per group. Bottom: daily measurements of primary tumor size. Values are mean ± SD. Statistical significance was determined by the two-tailed Student's t test. ***p < 0.001.

(D) Tumors from mice treated with ALW-II-41-27 or vehicle described in (D) were collected for H&E and assessed for Y588 p-EphA2, p-AKT, p-JAK1, and p-STAT3 expression by IHC. Scale bar 100 μm.

clathrin-mediated endocytosis to activate AKT and MAPK (Sigismund et al., 2008). Another RTK, c-MET, has been shown to need trafficking to a perinuclear endosome to activate STAT3 (Kermorgant and Parker, 2008). Thus, we hypothesize that EphA2 activation of JAK1/STAT3 might similarly depend on the perinuclear trafficking of EphA2 and JAK1. Taken together, our results show that EphA2 activates STAT3 by interacting with JAK1 and provides a potential approach to target STAT3 in HCC. Given the critical oncogenic roles of both EphA2 and STAT3 in many cancers, we suspect that the EphA2/JAK1/STAT3 axis is not limited to HCC. For example, previous studies provide independent evidence that either EphA2 or STAT3 is critical for glioma tumor progression and contribute to the glioma stem cell phenotype (Binda et al., 2012; Schaefer et al., 2002;

Sherry et al., 2009; Wykosky et al., 2005). The data regarding EphA2 and STAT3 in gliomas suggest that the two pathways might be connected in glioma tumors. Future studies should elucidate the connection between EphA2 and STAT3 in other cancers and explore the therapeutic potential of targeting EphA2, especially in cancers driven by the STAT3 pathway.

Considering the diverse biological functions of EphA2 signaling and the lack of understanding of its functions in HCC, further investigation of its role in HCC is warranted. In addition to the two pathways highlighted in this study, GSEA also revealed oncogenic pathways such as KRAS signaling and angiogenesis (Table S3A), which were regulated by EphA2 signaling in other cancers (Macrae et al., 2005; Sáinz-Jaspeado et al., 2013). Thus, we aim to investigate how EphA2 regulates these oncogenic pathways in HCC in our future studies.

Currently, several EphA2 therapeutics are in clinical trials for cancers in which the oncogenic function of EphA2 is well-established, such as breast cancer, melanoma, and glioblastoma (Boyd et al., 2014). However, a majority of therapies do not target EphA2 functions directly but use EphA2 as bait. For example, MM-310 is a modified EphA2-sensing nanoparticle that delivers docetaxel to EphA2-positive tumors. Although dasatinib has been investigated clinically as an EphA2 inhibitor, it primarily targets SRC and ABL (Gnoni et al., 2011). In this study, we demonstrated the therapeutic potential of targeting EphA2 in HCC by showing that a potent and selective EphA2 inhibitor (ALW-II-41-27) significantly suppresses tumor growth *in vitro* and *in vivo* models of HCC. Our findings support the clinical investigation to assess the safety and efficacy of EphA2 inhibitors such as ALW-II-41-27 in the treatment of advanced HCC, especially in patients showing activation of EphA2.

STAR★METHODS

Detailed methods are provided in the online version of this paper and include the following:

- KEY RESOURCES TABLE
- RESOURCE AVAILABILITY
  - Lead contact
  - Materials availiability
  - Data and code availiability
- EXPERIMENTAL MODEL AND SUBJECT DETAILS
  - Cell Lines
  - Mice Models
- METHOD DETAILS
  - Plasmids
  - TMA analysis
  - Western Blot Analysis
  - Immunohistochemistry and immunofluorescence
  - Transient transfection
  - Lentivirus particle production and transduction
  - Gene knockdown
  - Cell Viability Assays
  - High-resolution hepatic ultrasound
  - RNA isolation, RNA sequencing, dataset analysis, and qPCR
  - Proximity Ligation Assay
  - EFNA1-FC experiment
  - IL6 ELISA analysis
- QUANTIFICATION AND STATISTICAL ANALYSIS

SUPPLEMENTAL INFORMATION

Supplemental information can be found online at https://doi.org/10.1016/j.celrep.2021.108765.

ACKNOWLEDGMENTS

We thank Dr. Andrew Dingwall, Dr. Nancy Zeleznik-Le, and Dr. Jiwang Zhang for their helpful advice on this project. This work was supported by the American Cancer Society (RSG-18-107 to W.Q.) and the National Cancer Institute (R01CA197128 to W.Q. and P50CA210964 to Mayo Clinic Hepatobiliary SPORE). The content is solely the authors' responsibility and does not necessarily represent the official views of the American Cancer Society or the National Cancer Institute.

AUTHOR CONTRIBUTIONS

Conceptualization, H.W. and W.Q.; Methodology, H.W. and W.Q.; Formal Analysis, H.W., W.H., C.B., C.J., J.Y., J.L., X.D., and W.Q.; Investigation, H.W., W.H., A.P., C.B., J.R.B., and W.Q.; Writing – Original Draft, H.W. and W.Q.; Writing – Review & Editing, H.W., W.H., A.P., C.B., J.R.B., X.D, J.L., M.F.D., S.J.C., L.R.R., A.D., and W.Q.; Funding Acquisition, W.Q. and L.R.R.; Visualization, H.W. and W.Q.; Resources, M.F.D., F.A., L.R.R., and W.Q.; Supervision, W.Q.

DECLARATION OF INTERESTS

The authors declare no competing interests.

Received: February 11, 2020
Revised: December 7, 2020
Accepted: January 28, 2021
Published: February 23, 2021

REFERENCES

Abdelhamed, S., Ogura, K., Yokoyama, S., Saiki, I., and Hayakawa, Y. (2016). AKT-STAT3 Pathway as a Downstream Target of EGFR Signaling to Regulate PD-L1 Expression on NSCLC cells. J. Cancer *7*, 1579–1586.

Alessi, D.R., Andjelkovic, M., Caudwell, B., Cron, P., Morrice, N., Cohen, P., and Hemmings, B.A. (1996). Mechanism of activation of protein kinase B by insulin and IGF-1. EMBO J. *15*, 6541–6551.

Amato, K.R., Wang, S., Hastings, A.K., Youngblood, V.M., Santapuram, P.R., Chen, H., Cates, J.M., Colvin, D.C., Ye, F., Brantley-Sieders, D.M., et al. (2014). Genetic and pharmacologic inhibition of EPHA2 promotes apoptosis in NSCLC. J. Clin. Invest. *124*, 2037–2049.

Amato, K.R., Wang, S., Tan, L., Hastings, A.K., Song, W., Lovly, C.M., Meador, C.B., Ye, F., Lu, P., Balko, J.M., et al. (2016). EPHA2 Blockade Overcomes Acquired Resistance to EGFR Kinase Inhibitors in Lung Cancer. Cancer Res. *76*, 305–318.

Andl, C.D., Mizushima, T., Oyama, K., Bowser, M., Nakagawa, H., and Rustgi, A.K. (2004). EGFR-induced cell migration is mediated predominantly by the JAK-STAT pathway in primary esophageal keratinocytes. Am. J. Physiol. Gastrointest. Liver Physiol. *287*, G1227–G1237.

Bergmann, J., Müller, M., Baumann, N., Reichert, M., Heneweer, C., Bolik, J., Lücke, K., Gruber, S., Carambia, A., Boretius, S., et al. (2017). IL-6 trans-signaling is essential for the development of hepatocellular carcinoma in mice. Hepatology *65*, 89–103.

Binda, E., Visioli, A., Giani, F., Lamorte, G., Copetti, M., Pitter, K.L., Huse, J.T., Cajola, L., Zanetti, N., DiMeco, F., et al. (2012). The EphA2 receptor drives self-

renewal and tumorigenicity in stem-like tumor-propagating cells from human glioblastomas. Cancer Cell *22*, 765–780.

Binns, K.L., Taylor, P.P., Sicheri, F., Pawson, T., and Holland, S.J. (2000). Phosphorylation of Tyrosine Residues in the Kinase Domain and Juxtamembrane Region Regulates the Biological and Catalytic Activities of Eph Receptors. Mol. Cell Biol. *20*, 4791–4805.

Boissier, P., Chen, J., and Huynh-Do, U. (2013). EphA2 signaling following endocytosis: role of Tiam1. Traffic *14*, 1255–1271.

Boyd, A.W., Bartlett, P.F., and Lackmann, M. (2014). Therapeutic targeting of EPH receptors and their ligands. Nat. Rev. Drug Discov. *13*, 39–62.

Calvisi, D.F., Ladu, S., Gorden, A., Farina, M., Conner, E.A., Lee, J.S., Factor, V.M., and Thorgeirsson, S.S. (2006). Ubiquitous activation of Ras and Jak/Stat pathways in human HCC. Gastroenterology *130*, 1117–1128.

Chang, Q., Jorgensen, C., Pawson, T., and Hedley, D.W. (2008). Effects of dasatinib on EphA2 receptor tyrosine kinase activity and downstream signalling in pancreatic cancer. Br. J. Cancer *99*, 1074–1082.

Choi, Y., Syeda, F., Walker, J.R., Finerty, P.J., Jr., Cuerrier, D., Wojciechowski, A., Liu, Q., Dhe-Paganon, S., and Gray, N.S. (2009). Discovery and structural analysis of Eph receptor tyrosine kinase inhibitors. Bioorg. Med. Chem. Lett. *19*, 4467–4470.

Cieply, B., Zeng, G., Proverbs-Singh, T., Geller, D.A., and Monga, S.P.S. (2009). Unique phenotype of hepatocellular cancers with exon-3 mutations in beta-catenin gene. Hepatology *49*, 821–831.

Cong, L., Ran, F.A., Cox, D., Lin, S., Barretto, R., Habib, N., Hsu, P.D., Wu, X., Jiang, W., Marraffini, L.A., and Zhang, F. (2013). Multiplex genome engineering using CRISPR/Cas systems. Science *339*, 819–823.

Cui, X.-D., Lee, M.-J., Yu, G.-R., Kim, I.-H., Yu, H.-C., Song, E.-Y., and Kim, D.-G. (2010). EFNA1 ligand and its receptor EphA2: potential biomarkers for hepatocellular carcinoma. Int. J. Cancer *126*, 940–949.

Darnell, J.E., Jr., Kerr, I.M., and Stark, G.R. (1994). Jak-STAT pathways and transcriptional activation in response to IFNs and other extracellular signaling proteins. Science *264*, 1415–1421.

Fang, W.B., Brantley-Sieders, D.M., Hwang, Y., Ham, A.-J.L., and Chen, J. (2008). Identification and Functional Analysis of Phosphorylated Tyrosine Residues within EphA2 Receptor Tyrosine Kinase. J. Biol. Chem. *283*, 16017–16026.

Ferguson, F.M., and Gray, N.S. (2018). Kinase inhibitors: the road ahead. Nat. Rev. Drug Discov. *17*, 353–377.

Ferlay, J., Soerjomataram, I., Dikshit, R., Eser, S., Mathers, C., Rebelo, M., Parkin, D.M., Forman, D., and Bray, F. (2015). Cancer incidence and mortality worldwide: sources, methods and major patterns in GLOBOCAN 2012. Int. J. Cancer *136*, E359–E386.

Finn, R.S., Qin, S., Ikeda, M., Galle, P.R., Ducreux, M., Kim, T.Y., Kudo, M., Breder, V., Merle, P., Kaseb, A.O., et al.; IMbrave150 Investigators (2020). Atezolizumab plus Bevacizumab in Unresectable Hepatocellular Carcinoma. N. Engl. J. Med. *382*, 1894–1905.

Galicia, V.A., He, L., Dang, H., Kanel, G., Vendryes, C., French, B.A., Zeng, N., Bayan, J.A., Ding, W., Wang, K.S., et al. (2010). Expansion of hepatic tumor progenitor cells in Pten-null mice requires liver injury and is reversed by loss of AKT2. Gastroenterology *139*, 2170–2182.

Gnoni, A., Marech, I., Silvestris, N., Vacca, A., and Lorusso, V. (2011). Dasatinib: an anti-tumour agent via Src inhibition. Curr. Drug Targets *12*, 563–578.

Grabinski, N., Ewald, F., Hofmann, B.T., Staufer, K., Schumacher, U., Nashan, B., and Jücker, M. (2012). Combined targeting of AKT and mTOR synergistically inhibits proliferation of hepatocellular carcinoma cells. Mol. Cancer *11*, 85.

Haigis, K.M., Cichowski, K., and Elledge, S.J. (2019). Tissue-specificity in cancer: The rule, not the exception. Science *363*, 1150–1151.

Hall, J., Guo, G., Wray, J., Eyres, I., Nichols, J., Grotewold, L., Morfopoulou, S., Humphreys, P., Mansfield, W., Walker, R., et al. (2009). Oct4 and LIF/Stat3 additively induce Krüppel factors to sustain embryonic stem cell self-renewal. Cell Stem Cell *5*, 597–609.

He, G., and Karin, M. (2011). NF-κB and STAT3 - key players in liver inflammation and cancer. Cell Res. *21*, 159–168.

He, G., Yu, G.-Y., Temkin, V., Ogata, H., Kuntzen, C., Sakurai, T., Sieghart, W., Peck-Radosavljevic, M., Leffert, H.L., and Karin, M. (2010a). Hepatocyte IKK-beta/NF-kappaB inhibits tumor promotion and progression by preventing oxidative stress-driven STAT3 activation. Cancer Cell *17*, 286–297.

Himanen, J.P., Yermekbayeva, L., Janes, P.W., Walker, J.R., Xu, K., Atapattu, L., Rajashankar, K.R., Mensinga, A., Lackmann, M., Nikolov, D.B., and Dhe-Paganon, S. (2010). Architecture of Eph receptor clusters. Proc. Natl. Acad. Sci. USA *107*, 10860–10865.

Hirai, H., Maru, Y., Hagiwara, K., Nishida, J., and Takaku, F. (1987). A novel putative tyrosine kinase receptor encoded by the eph gene. Science *238*, 1717–1720.

Hochgräfe, F., Zhang, L., O'Toole, S.A., Browne, B.C., Pinese, M., Porta Cubas, A., Lehrbach, G.M., Croucher, D.R., Rickwood, D., Boulghourjian, A., et al. (2010). Tyrosine phosphorylation profiling reveals the signaling network characteristics of Basal breast cancer cells. Cancer Res. *70*, 9391–9401.

Horwitz, E., Stein, I., Andreozzi, M., Nemeth, J., Shoham, A., Pappo, O., Schweitzer, N., Tornillo, L., Kanarek, N., Quagliata, L., et al. (2014). Human and mouse VEGFA-amplified hepatocellular carcinomas are highly sensitive to sorafenib treatment. Cancer Discov. *4*, 730–743.

Huynh, J., Chand, A., Gough, D., and Ernst, M. (2019). Therapeutically exploiting STAT3 activity in cancer - using tissue repair as a road map. Nat. Rev. Cancer *19*, 82–96.

Johnson, D.E., O'Keefe, R.A., and Grandis, J.R. (2018). Targeting the IL-6/JAK/STAT3 signalling axis in cancer. Nat. Rev. Clin. Oncol. *15*, 234–248.

Kania, A., and Klein, R. (2016). Mechanisms of ephrin-Eph signalling in development, physiology and disease. Nat. Rev. Mol. Cell Biol. *17*, 240–256.

Kaposi-Novak, P., Lee, J.-S., Gòmez-Quiroz, L., Coulouarn, C., Factor, V.M., and Thorgeirsson, S.S. (2006). Met-regulated expression signature defines a subset of human hepatocellular carcinomas with poor prognosis and aggressive phenotype. J. Clin. Invest. *116*, 1582–1595.

Kermorgant, S., and Parker, P.J. (2008). Receptor trafficking controls weak signal delivery: a strategy used by c-Met for STAT3 nuclear accumulation. J. Cell Biol. *182*, 855–863.

Khanna, C., Wan, X., Bose, S., Cassaday, R., Olomu, O., Mendoza, A., Yeung, C., Gorlick, R., Hewitt, S.M., and Helman, L.J. (2004). The membrane-cytoskeleton linker ezrin is necessary for osteosarcoma metastasis. Nat. Med. *10*, 182–186.

Lai, K.-O., Chen, Y., Po, H.-M., Lok, K.-C., Gong, K., and Ip, N.Y. (2004). Identification of the Jak/Stat proteins as novel downstream targets of EphA4 signaling in muscle: implications in the regulation of acetylcholinesterase expression. J. Biol. Chem. *279*, 13383–13392.

Leonard, W.J., and O'Shea, J.J. (1998). Jaks and STATs: biological implications. Annu. Rev. Immunol. *16*, 293–322.

Leung, C.O.N., Tong, M., Chung, K.P.S., Zhou, L., Che, N., Tang, K.H., Ding, J., Lau, E.Y.T., Ng, I.O.L., Ma, S., and Lee, T.K.W. (2020). Overriding Adaptive Resistance to Sorafenib Through Combination Therapy With Src Homology 2 Domain-Containing Phosphatase 2 Blockade in Hepatocellular Carcinoma. Hepatology *72*, 155–168.

Li, W.C., Ye, S.L., Sun, R.X., Liu, Y.K., Tang, Z.Y., Kim, Y., Karras, J.G., and Zhang, H. (2006). Inhibition of growth and metastasis of human hepatocellular carcinoma by antisense oligonucleotide targeting signal transducer and activator of transcription 3. Clin. Cancer Res. *12*, 7140–7148.

Li, H., Sun, Q., Han, B., Yu, X., Hu, B., and Hu, S. (2015). MiR-26b inhibits hepatocellular carcinoma cell proliferation, migration, and invasion by targeting EphA2. Int. J. Clin. Exp. Pathol. *8*, 4782–4790.

Llovet, J.M. (2014). Focal gains of VEGFA: candidate predictors of sorafenib response in hepatocellular carcinoma. Cancer Cell *25*, 560–562.

Llovet, J.M., Ricci, S., Mazzaferro, V., Hilgard, P., Gane, E., Blanc, J.-F., de Oliveira, A.C., Santoro, A., Raoul, J.-L., Forner, A., et al.; SHARP Investigators Study Group (2008). Sorafenib in advanced hepatocellular carcinoma. N. Engl. J. Med. *359*, 378–390.

Llovet, J.M., Villanueva, A., Lachenmayer, A., and Finn, R.S. (2015). Advances in targeted therapies for hepatocellular carcinoma in the genomic era. Nat. Rev. Clin. Oncol. *12*, 408–424.

Lokau, J., Schoeder, V., Haybaeck, J., and Garbers, C. (2019). Jak-Stat Signaling Induced by Interleukin-6 Family Cytokines in Hepatocellular Carcinoma. Cancers (Basel) *11*, 1704.

Macrae, M., Neve, R.M., Rodriguez-Viciana, P., Haqq, C., Yeh, J., Chen, C., Gray, J.W., and McCormick, F. (2005). A conditional feedback loop regulates Ras activity through EphA2. Cancer Cell *8*, 111–118.

Markosyan, N., Li, J., Sun, Y.H., Richman, L.P., Lin, J.H., Yan, F., Quinones, L., Sela, Y., Yamazoe, T., Gordon, N., et al. (2019). Tumor cell-intrinsic EPHA2 suppresses anti-tumor immunity by regulating PTGS2 (COX-2). J. Clin. Invest. *129*, 3594–3609.

Martini, G., Cardone, C., Vitiello, P.P., Belli, V., Napolitano, S., Troiani, T., Ciardiello, D., Della Corte, C.M., Morgillo, F., Matrone, N., et al. (2019). EPHA2 Is a Predictive Biomarker of Resistance and a Potential Therapeutic Target for Improving Antiepidermal Growth Factor Receptor Therapy in Colorectal Cancer. Mol. Cancer Ther. *18*, 845–855.

Matter, M.S., Decaens, T., Andersen, J.B., and Thorgeirsson, S.S. (2014). Targeting the mTOR pathway in hepatocellular carcinoma: current state and future trends. J. Hepatol. *60*, 855–865.

Miao, H., Li, D.-Q., Mukherjee, A., Guo, H., Petty, A., Cutter, J., Basilion, J.P., Sedor, J., Wu, J., Danielpour, D., et al. (2009). EphA2 mediates ligand-dependent inhibition and ligand-independent promotion of cell migration and invasion via a reciprocal regulatory loop with Akt. Cancer Cell *16*, 9–20.

Miao, H., Gale, N.W., Guo, H., Qian, J., Petty, A., Kaspar, J., Murphy, A.J., Valenzuela, D.M., Yancopoulos, G., Hambardzumyan, D., et al. (2015). EphA2 promotes infiltrative invasion of glioma stem cells in vivo through cross-talk with Akt and regulates stem cell properties. Oncogene *34*, 558–567.

Murase, S. (2013). Signal transducer and activator of transcription 3 (STAT3) degradation by proteasome controls a developmental switch in neurotrophin dependence. J. Biol. Chem. *288*, 20151–20161.

Park, O.K., Schaefer, L.K., Wang, W., and Schaefer, T.S. (2000). Dimer stability as a determinant of differential DNA binding activity of Stat3 isoforms. J. Biol. Chem. *275*, 32244–32249.

Pasquale, E.B. (2010). Eph receptors and ephrins in cancer: bidirectional signalling and beyond. Nat. Rev. Cancer *10*, 165–180.

Patil, M.A., Lee, S.A., Macias, E., Lam, E.T., Xu, C., Jones, K.D., Ho, C., Rodriguez-Puebla, M., and Chen, X. (2009). Role of cyclin D1 as a mediator of c-Met- and beta-catenin-induced hepatocarcinogenesis. Cancer Res. *69*, 253–261.

Qin, X.-F., An, D.S., Chen, I.S.Y., and Baltimore, D. (2003). Inhibiting HIV-1 infection in human T cells by lentiviral-mediated delivery of small interfering RNA against CCR5. Proc. Natl. Acad. Sci. USA *100*, 183–188.

Roessler, S., Jia, H.L., Budhu, A., Forgues, M., Ye, Q.H., Lee, J.S., Thorgeirsson, S.S., Sun, Z., Tang, Z.Y., Qin, L.X., and Wang, X.W. (2010). A unique metastasis gene signature enables prediction of tumor relapse in early-stage hepatocellular carcinoma patients. Cancer Res. *70*, 10202–10212.

Sabet, O., Stockert, R., Xouri, G., Brüggemann, Y., Stanoev, A., and Bastiaens, P.I.H. (2015). Ubiquitination switches EphA2 vesicular traffic from a continuous safeguard to a finite signalling mode. Nat. Commun. *6*, 8047.

Sáinz-Jaspeado, M., Huertas-Martinez, J., Lagares-Tena, L., Martin Liberal, J., Mateo-Lozano, S., de Alava, E., de Torres, C., Mora, J., Del Muro, X.G., and Tirado, O.M. (2013). EphA2-induced angiogenesis in ewing sarcoma cells works through bFGF production and is dependent on caveolin-1. PLoS ONE *8*, e71449.

Salaita, K., Nair, P.M., Petit, R.S., Neve, R.M., Das, D., Gray, J.W., and Groves, J.T. (2010). Restriction of receptor movement alters cellular response: physical force sensing by EphA2. Science *327*, 1380–1385.

Schaefer, L.K., Ren, Z., Fuller, G.N., and Schaefer, T.S. (2002). Constitutive activation of Stat3α in brain tumors: localization to tumor endothelial cells and activation by the endothelial tyrosine kinase receptor (VEGFR-2). Oncogene *21*, 2058–2065.

Schroeder, A., Herrmann, A., Cherryholmes, G., Kowolik, C., Buettner, R., Pal, S., Yu, H., Müller-Newen, G., and Jove, R. (2014). Loss of androgen receptor expression promotes a stem-like cell phenotype in prostate cancer through STAT3 signaling. Cancer Res. *74*, 1227–1237.

Sebestyén, M.G., Budker, V.G., Budker, T., Subbotin, V.M., Zhang, G., Monahan, S.D., Lewis, D.L., Wong, S.C., Hagstrom, J.E., and Wolff, J.A. (2006). Mechanism of plasmid delivery by hydrodynamic tail vein injection. I. Hepatocyte uptake of various molecules. J. Gene Med. *8*, 852–873.

Shang, N., Arteaga, M., Zaidi, A., Stauffer, J., Cotler, S.J., Zeleznik-Le, N.J., Zhang, J., and Qiu, W. (2015). FAK is required for c-Met/β-catenin-driven hepatocarcinogenesis. Hepatology *61*, 214–226.

Shang, N., Wang, H., Bank, T., Perera, A., Joyce, C., Kuffel, G., Zilliox, M.J., Cotler, S.J., Ding, X., Dhanarajan, A., et al. (2019). Focal Adhesion Kinase and β-Catenin Cooperate to Induce Hepatocellular Carcinoma. Hepatology *70*, 1631–1645.

Sherry, M.M., Reeves, A., Wu, J.K., and Cochran, B.H. (2009). STAT3 is required for proliferation and maintenance of multipotency in glioblastoma stem cells. Stem Cells *27*, 2383–2392.

Sigismund, S., Argenzio, E., Tosoni, D., Cavallaro, E., Polo, S., and Di Fiore, P.P. (2008). Clathrin-mediated internalization is essential for sustained EGFR signaling but dispensable for degradation. Dev. Cell *15*, 209–219.

Sinnberg, T., Makino, E., Krueger, M.A., Velic, A., Macek, B., Rothbauer, U., Groll, N., Pötz, O., Czemmel, S., Niessner, H., et al. (2016). A Nexus Consisting of Beta-Catenin and Stat3 Attenuates BRAF Inhibitor Efficacy and Mediates Acquired Resistance to Vemurafenib. EBioMedicine *8*, 132–149.

Söderberg, O., Gullberg, M., Jarvius, M., Ridderstråle, K., Leuchowius, K.-J., Jarvius, J., Wester, K., Hydbring, P., Bahram, F., Larsson, L.-G., and Landegren, U. (2006). Direct observation of individual endogenous protein complexes in situ by proximity ligation. Nat. Methods *3*, 995–1000.

Song, W., Hwang, Y., Youngblood, V.M., Cook, R.S., Balko, J.M., Chen, J., and Brantley-Sieders, D.M. (2017). Targeting EphA2 impairs cell cycle progression and growth of basal-like/triple-negative breast cancers. Oncogene *36*, 5620–5630.

Song, M., Bode, A.M., Dong, Z., and Lee, M.H. (2019). AKT as a Therapeutic Target for Cancer. Cancer Res. *79*, 1019–1031.

Stark, G.R., Kerr, I.M., Williams, B.R., Silverman, R.H., and Schreiber, R.D. (1998). How cells respond to interferons. Annu. Rev. Biochem. *67*, 227–264.

Stauffer, J.K., Scarzello, A.J., Andersen, J.B., De Kluyver, R.L., Back, T.C., Weiss, J.M., Thorgeirsson, S.S., and Wiltrout, R.H. (2011). Coactivation of AKT and β-catenin in mice rapidly induces formation of lipogenic liver tumors. Cancer Res. *71*, 2718–2727.

Stewart, S.A., Dykxhoorn, D.M., Palliser, D., Mizuno, H., Yu, E.Y., An, D.S., Sabatini, D.M., Chen, I.S.Y., Hahn, W.C., Sharp, P.A., et al. (2003). Lentivirus-delivered stable gene silencing by RNAi in primary cells. RNA *9*, 493–501.

Swidergall, M., Solis, N.V., Lionakis, M.S., and Filler, S.G. (2018). EphA2 is an epithelial cell pattern recognition receptor for fungal β-glucans. Nat. Microbiol. *3*, 53–61.

Tang, Z., Li, C., Kang, B., Gao, G., Li, C., and Zhang, Z. (2017). GEPIA: a web server for cancer and normal gene expression profiling and interactive analyses. Nucleic Acids Res. *45* (*W1*), W98–W102.

Tao, J., Xu, E., Zhao, Y., Singh, S., Li, X., Couchy, G., Chen, X., Zucman-Rossi, J., Chikina, M., and Monga, S.P.S. (2016). Modeling a human hepatocellular carcinoma subset in mice through coexpression of met and point-mutant β-catenin. Hepatology *64*, 1587–1605.

Thompson, J.E., Cubbon, R.M., Cummings, R.T., Wicker, L.S., Frankshun, R., Cunningham, B.R., Cameron, P.M., Meinke, P.T., Liverton, N., Weng, Y., and DeMartino, J.A. (2002). Photochemical preparation of a pyridone containing tetracycle: a Jak protein kinase inhibitor. Bioorg. Med. Chem. Lett. *12*, 1219–1223.

Tward, A.D., Jones, K.D., Yant, S., Cheung, S.T., Fan, S.T., Chen, X., Kay, M.A., Wang, R., and Bishop, J.M. (2007). Distinct pathways of genomic progression to benign and malignant tumors of the liver. Proc. Natl. Acad. Sci. USA *104*, 14771–14776.

Villanueva, A. (2019). Hepatocellular Carcinoma. N. Engl. J. Med. *380*, 1450–1462.

Villanueva, A., Chiang, D.Y., Newell, P., Peix, J., Thung, S., Alsinet, C., Tovar, V., Roayaie, S., Minguez, B., Sole, M., et al. (2008). Pivotal role of mTOR signaling in hepatocellular carcinoma. Gastroenterology *135*, 1972–1983.

Wang, F., Bank, T., Malnassy, G., Arteaga, M., Shang, N., Dalheim, A., Ding, X., Cotler, S.J., Denning, M.F., Nishimura, M.I., et al. (2018). Inhibition of insulin-like growth factor 1 receptor enhances the efficacy of sorafenib in inhibiting hepatocellular carcinoma cell growth and survival. Hepatol. Commun. *2*, 732–746.

Weibrecht, I., Leuchowius, K.-J., Clausson, C.-M., Conze, T., Jarvius, M., Howell, W.M., Kamali-Moghaddam, M., and Söderberg, O. (2010). Proximity ligation assays: a recent addition to the proteomics toolbox. Expert Rev. Proteomics *7*, 401–409.

Wong, A.L.A., Hirpara, J.L., Pervaiz, S., Eu, J.-Q., Sethi, G., and Goh, B.-C. (2017). Do STAT3 inhibitors have potential in the future for cancer therapy? Expert Opin. Investig. Drugs *26*, 883–887.

Wykosky, J., and Debinski, W. (2008). The EphA2 receptor and ephrinA1 ligand in solid tumors: function and therapeutic targeting. Mol. Cancer Res. *6*, 1795–1806.

Wykosky, J., Gibo, D.M., Stanton, C., and Debinski, W. (2005). EphA2 as a novel molecular marker and target in glioblastoma multiforme. Mol. Cancer Res. *3*, 541–551.

Xiang, Y., Huang, Y., Sun, H., Pan, Y., Wu, M., and Zhang, J. (2019). Deregulation of miR-520d-3p promotes hepatocellular carcinoma development via lncRNA MIAT regulation and EPHA2 signaling activation. Biomed. Pharmacother. *109*, 1630–1639.

Xue, W., Chen, S., Yin, H., Tammela, T., Papagiannakopoulos, T., Joshi, N.S., Cai, W., Yang, G., Bronson, R., Crowley, D.G., et al. (2014). CRISPR-mediated direct mutation of cancer genes in the mouse liver. Nature *514*, 380–384.

Yadav, V., and Denning, M.F. (2011). Fyn is induced by Ras/PI3K/Akt signaling and is required for enhanced invasion/migration. Mol. Carcinog. *50*, 346–352.

Yang, P., Yuan, W., He, J., Wang, J., Yu, L., Jin, X., Hu, Y., Liao, M., Chen, Z., and Zhang, Y. (2009). Overexpression of EphA2, MMP-9, and MVD-CD34 in hepatocellular carcinoma: Implications for tumor progression and prognosis. Hepatol. Res. *39*, 1169–1177.

Yang, X., Boehm, J.S., Yang, X., Salehi-Ashtiani, K., Hao, T., Shen, Y., Lubonja, R., Thomas, S.R., Alkan, O., Bhimdi, T., et al. (2011). A public genome-scale lentiviral expression library of human ORFs. Nat. Methods *8*, 659–661.

Yokogami, K., Wakisaka, S., Avruch, J., and Reeves, S.A. (2000). Serine phosphorylation and maximal activation of STAT3 during CNTF signaling is mediated by the rapamycin target mTOR. Curr. Biol. *10*, 47–50.

Yu, H., Lee, H., Herrmann, A., Buettner, R., and Jove, R. (2014). Revisiting STAT3 signalling in cancer: new and unexpected biological functions. Nat. Rev. Cancer *14*, 736–746.

Zelinski, D.P., Zantek, N.D., Stewart, J.C., Irizarry, A.R., and Kinch, M.S. (2001). EphA2 overexpression causes tumorigenesis of mammary epithelial cells. Cancer Res. *61*, 2301–2306.

STAR★METHODS

KEY RESOURCES TABLE

REAGENT or RESOURCE	SOURCE	IDENTIFIER
Antibodies		
EphA2 (C-3)	Santa Cruz	sc-398832
EphA2 (phospho Y588) (D7X2L)	Cell signaling	12677S; RRID:AB_2797989
EphA2 (phospho S897) (D9A1)	Cell signaling	6347S; RRID:AB_11220420
Goat anti-Mouse IgG (H+L) Cross-Adsorbed Secondary Antibody	Thermo Fisher Scientific	31432; RRID:AB_228302
Goat anti-Rabbit IgG (H+L) Cross-Adsorbed Secondary Antibody	Thermo Fisher Scientific	31462; RRID:AB_228338
Goat anti-Rabbit IgG (H+L) Cross-Adsorbed Secondary Antibody, Biotin	Thermo Fisher Scientific	31822; RRID:AB_228337
Goat anti-Mouse IgG (H+L) Cross-Adsorbed Secondary Antibody, Biotin	Thermo Fisher Scientific	31802; RRID:AB_228301
AKT (phospho S473) (D9E)	Cell signaling	4060S; RRID:AB_2315049
AKT (phospho T308) (244F9)	Cell signaling	4056S; RRID:AB_331163
AKT	Cell signaling	9272S; RRID:AB_329827
β-Actin	Sigma-Aldrich	A5441; RRID:AB_476744
GADPH (GA1R)	Thermo Fisher Scientific	MA5-15738; RRID:AB_10977387
GP130	R&D	MAB2281; RRID:AB_2296041
STAT3 (phospho Y705) (D3A7)	Cell signaling	9145S; RRID:AB_2491009
STAT3 (124H6)	Cell signaling	9139; RRID:AB_331757
MET (D1C2)	Cell signaling	8198; RRID:AB_10858224
β-Catenin	BD Biosciences	610153; RRID:AB_397554
Goat anti-Mouse IgG (H+L) Cross-Adsorbed Secondary Antibody, Alexa Fluor 488	Thermo Fisher Scientific	A-11001, RRID:AB_2534069
Goat anti-Rabbit IgG (H+L) Highly Cross-Adsorbed Secondary Antibody, Alexa Fluor 594	Thermo Fisher Scientific	A-11037; RRID:AB_2534095
Alpha-1-Fetoprotein Pathology Antibody	Agilent	A0008; RRID:AB_2650473
Ki-67 (D3B5)	Cell signaling	12202; RRID:AB_2620142
JAK1 (phospho Y1034/1035) (D7N4Z)	Cell signaling	74129; RRID:AB_2799851
Jak1 (6G4)	Cell signaling	3344, RRID:AB_2265054
Bacterial and virus strains		
MAX Efficiency Stbl2 Competent Cells	Thermo Fisher Scientific	10268019
MAX Efficiency DH5α Competent Cells	Thermo Fisher Scientific	18258012
Biological samples		
Normal + HCC human liver samples	Mayo Clinic Rochester; Dr. Lewis R. Roberts	https://www.cancer.gov/about-nci/organization/ccg/research/structural-genomics/tcga
Chemicals, peptides, and recombinant proteins		
ALW-II-41-27	APExBIO	A3165
Critical commercial assays		
AlamarBlue®	BIO-RAD	BUF012B
GeneJET Endo-Free Plasmid Maxiprep Kit	Thermo Fisher Scientific	K0861
RNeasy Mini Kit	QIAGEN	74106
Duolink® *In Situ* Red Starter Kit Mouse/Rabbit	Millipore Sigma	DUO92101

(*Continued on next page*)

Continued

REAGENT or RESOURCE	SOURCE	IDENTIFIER
Deposited data		
RNaseq EphA2 knockdown	This Paper	Database: GEO, GSE141880
RNaseq expression analysis of HCC and normal liver tissue	Database: TCGA	https://www.cancer.gov/about-nci/organization/ccg/research/structural-genomics/tcga
Experimental models: cell lines		
Huh7	JCRB	JCRB0403
Hep3B	ATCC	HB-8064
PLC/PRF/5	ATCC	CRL-8024
SNU387	ATCC	CRL-2237
SNU423	ATCC	CRL-2238
SNU449	ATCC	CRL-2234
SNU475	ATCC	CRL-2236
Experimental models: organisms/strains		
NSG-A2	Jackson Laboratory	009617
C57BL/6	Jackson Laboratory	000664
Oligonucleotides		
Primer sequences for qRT-PCR	Table S3B	N/A
Human EphA2 shRNAshEphA2-1: CCGGCCATCAAGATGCAGCAGTATACTCGAGTATACTGCTG CATCTTGATGGTTTTTG	Millipore Sigma	TRCN0000231647
Human EphA2 shRNAshEphA2-2: CCGGGATAAGTTTCTATTCTGTCAGCTCGAGCTGACAGAATA GAAACTTATCTTTTTG	Millipore Sigma	TRCN0000195734
Human EphA2 shRNAshEphA2-5: CCGGTCGGACAGACATATAGGATATCTCGAGATATCCTATAT GTCTGTCCGATTTTTG	Millipore Sigma	TRCN0000231648
Human JAK1: siGENOME SMARTpool siRNA	Dharmacon/Horizon	SO-2796483G
Human JAK1: CCACAUAGCUGAUCUGAAA	Dharmacon/Horizon	D-003145-05
Human JAK1: UGAAAUCACUCACAUUGUA	Dharmacon/Horizon	D-003145-06
Human JAK1: UAAGGAACCUCUAUCAUGA	Dharmacon/Horizon	D-003145-07
Human JAK1: GCAGGUGGCUGUUAAAUCU	Dharmacon/Horizon	D-003145-08
Mouse EphA2 sgRNAsgEphA2-1: CAACGTGGTATCCGGCGACC	Dr. Feng Zhang; Cong et al., 2013	MGLibA_16318
Mouse EphA2 sgRNAsgEphA2-2: TTCGCTGTCGAAGCACGCAA	Dr. Feng Zhang; Cong et al., 2013	MGLibA_16319
Mouse EphA2 sgRNAsgEphA2-3: CTGCTGACCGTGATCTCGTC	Dr. Feng Zhang; Cong et al., 2013	MGLibA_16320
Recombinant DNA		
pCMV-dR8.2 dvpr	Stewart et al., 2003	8455; RRID:Addgene_8455
pCMV-VSV-G	Stewart et al., 2003	8454; RRID:Addgene_8454
pLKO.1-puro-shEphA2-1	Millipore Sigma	TRCN0000231647
pLKO.1-puro-shEphA2-2	Millipore Sigma	TRCN0000195734
pLKO.1-puro-shEphA2-5	Millipore Sigma	TRCN0000231648
FG12	Qin et al., 2003	14884; RRID:Addgene_14884
FG12-CMV-CA-AKT	Dr. Mitchell Denning, LUC	Yadav and Denning, 2011
pMD2.G	Dr. Didier Trono	12259; RRID:Addgene_12259
pLX304	Yang et al., 2011	RRID:Addgene_25890
pEXP304-STAT3/V5	Sinnberg et al., 2016; DNASU	HsCD00443857; PMID: 27428425
pEXP304-FLAG/V5	Dr. Takashi Shimamura, UIC	N/A
pT3-CAT	Khanna et al., 2004; Shang et al., 2015	N/A

(*Continued on next page*)

Continued

REAGENT or RESOURCE	SOURCE	IDENTIFIER
pT3-MET	Khanna et al., 2004; Shang et al., 2015	N/A
pT3-GFP	Shang et al., 2015	N/A
pT3-EphA2	This Paper	N/A
pX330-U6-Chimeric_BB-CBh-hSpCas9 (PX330)	Dr. Feng Zhang; Cong et al., 2013	Addgene plasmid # 42230; RRID:Addgene_42230
pX330-sgEphA2-1	This Paper	N/A
pX330-sgEphA2-2	This Paper	N/A
pX330-sgEphA2-3	This Paper	N/A
Software and algorithms		
PRISM	GraphPad Software	Version 7
GEPIA	Tang et al., 2017	http://gepia.cancer-pku.cn/
ImageJ	NIH	https://imagej.nih.gov/ij/
GSEA	Broad Institute	http://www.gsea-msigdb.org/gsea/index.jsp
Bitplane Imaris	Oxford Instruments	https://imaris.oxinst.com/packages

RESOURCE AVAILABILITY

Lead contact

The lead contact for this manuscript is Dr. Wei Qiu (wqiu@luc.edu).

Materials availiability

Further information and requests for resources generated in this study should be directed to and will be fulfilled by the lead contact.

Data and code availiability

The datasets and code utilized in this study are available at GEO: GSE141880.

EXPERIMENTAL MODEL AND SUBJECT DETAILS

Cell Lines

HCC Cell lines were acquired from the American Type Culture Collection (ATCC®) or the Japanese Cancer Research Resources Bank (JCRB). Huh7, Hep3B, and PLC/PRF/5 were maintained in Dulbecco's modified Eagle's (DMEM) high glucose medium (Thermo Scientific, Waltham, MA) supplemented with 10% fetal bovine serum (Tissue Culture Biologicals), penicillin/streptomycin (Sigma-Aldrich, St. Louis, MO) in a humidified atmosphere of 5% CO2 at 37°C. SNU387, SNU423, SNU449, and SNU475 were cultured in RPMI 1640 supplemented with 10% fetal bovine serum (Tissue Culture Biologicals), 1x penicillin/streptomycin (Sigma-Aldrich, St. Louis, MO) at 37°C and 5% CO2.

Mice Models

All animals received humane care according to the "Guide for the Care and Use of Laboratory Animals" (https://login.archer.luhs.org/login?qurl=http://oacu.od.nih.gov%2fac_cbt%2fguide3.htm). All animal procedures were approved by the Institutional Animal Care and Use Committee at Loyola University Chicago. The mice were housed in micro-isolator cages in a room illuminated from 7:00 AM to 7:00 PM (12:12-hr light-dark cycle) and allowed access to water and chow *ad libitum*.

For xenograft studies: NSG-A2 mice were purchased from Jackson Laboratory. Mice were all 8 – 10 weeks old, 1:1 males to female, and evenly distributed in the experimental and control groups. For the *EphA2* knockdown and AKT and STAT3 rescue studies, $3x10^6$ cells were injected into the right and/or left flank of the mice (depending on the experiment). Mice were monitored for tumor growth by a digital caliper. Growth volume was calculated as volume = length × $width^2/2$. The tumor was extracted for the analysis described in the paper. The ALW-II-41-27 study method was adopted by Dr. Jin Chen Lab (Vanderbilt) (Song et al., 2017). $5x10^6$ cells were injected into the right flank of the mice. When the tumor reached $\geq$ 200 mm^3 at day 10, mice were treated with 15 mg/kg of ALW-II-41-27 dissolved in 10%1-methyl-2-pyrrolidinone, and 90% polyethylene glycol 300 (Sigma) injected intraperitoneally once daily for seven days. Tumors were measured daily, and tumor volume was calculated as described previously.

C57BL/6 mice were purchased from Jackson Laboratory the *in vivo* CRISPR and MET/CAT HCC models. Mice were all 8 – 10 weeks old, 1:1 male to female, and evenly distributed in experimental and control groups. To examine whether EphA2 is activated in the MET/CAT model (Shang et al., 2015), 50 μg of total plasmids, encoding the Sleeping Beauty transposase (HSB2) and transposons with oncogenes MET/CAT (22.5μg pT3-EF1α-c-MET(human) + 22.5μg pT3-EF1α-ΔN90-β-catenin (human)+ 5μg HSB2) (Shang et al., 2015), were injected hydrodynamically into age- and sex-matched mice. Mice were maintained on the standard diet and euthanized after seven weeks, and livers were collected for analysis. To knockout EphA2 in the MET/CAT-induced HCC model, age-and-sex-matched C57BL/6J mice were divided into two groups: one received MET/CAT + PX330 control, while the other received MET/CAT+ sgEphA2-2. 72.5 μg of total plasmids was dissolved in 2 mL of 0.9% saline and hydrodynamically injected in each mouse. The plasmids encode the single vector PX330-sgEphA2-CRISPR CAS9 (sgEphA2) or pX330-U6-Chimeric_BB-CBh-hSpCas9 (PX330, empty vector control), Sleeping Beauty transposase (HSB2) and transposons with oncogenes MET/CAT (22.5μg sgEphA2 or 22.5 μg PX330 + 22.5μg pT3-EF1α-c-MET(human) + 22.5μg pT3-EF1α-ΔN90-β-catenin (human) + 5 μg HSB2). Mice were monitored for approximately 6-9 weeks total as this is the average period for MET/CAT mice to develop end-stage HCC symptoms, including ascites and liver failure. Mice were then euthanized, and livers were collected for analysis.

METHOD DETAILS

Plasmids

The plasmids pT3-internal ribosome entry site (IRES) - green fluorescent protein (GFP), pT3-CAT, and pT3-MET and pT3-EphA2 were generated by Gateway cloning (Shang et al., 2015). sgEphA2-1, sgEphA2-2, and sgEphA3 target sequences were designed based on library and protocol from Feng Zhang Lab (Cong et al., 2013), and the final plasmids pX330-sgEphA2-1, pX330-sgEphA2-2, pX330-sgEphA2-3 were constructed by cloning *EphA2*-target sequences into pX330-U6-Chimeric_BB-CBh-hSpCas9 backbone following the protocol from Feng Zhang Lab (Cong et al., 2013). The plasmids were purified using the GeneJET Plasmid Maxiprep Kit (Thermo Fisher Scientific) for hydrodynamic tail vein injection.

The following plasmids were purchased: pCMV-dR8.2 dvpr (Addgene, #8455). pCMV-VSV-G (Addgene, #8454), pLKO.1-puro-shEphA2-1(Millipore Sigma, TRCN0000231647), pLKO.1-puro-shEphA2-2 (Millipore Sigma, TRCN0000195734), pLKO.1-puro-shEphA2-5 (Millipore Sigma, TRCN0000231648), FG12 (Addgene, #14884), pMD2.G (Addgene, #12259), pEXP304-STAT3/V5 (DNASU, HsCD00443857). The pEXP304-FLAG/V5 plasmid was generously donated from Dr. Takashi Shimamura (University of Illinois Chicago).

TMA analysis

IHC was performed as previously described (Shang et al., 2015). Human tissue microarrays (TMAs) were obtained from the Mayo Clinic. 153 cases of HCC and 63 non-tumor liver tissues (free of significant pathologies) were analyzed. The source of patients, demographic information, and their clinical presentations are shown in Table S1. An IRB (#707-03) was approved by the Mayo Clinic for this study. We summarized categorical data as frequency counts and percentages, and continuous measures as means, standard deviations, medians, and ranges. Categorical variables were compared using the chi-square test or Fisher's exact test. Continuous variables were compared using the one-way ANOVA test or Kruskal–Wallis test.

Western Blot Analysis

Cells/tissue lysate was prepared in RIPA lysis, and extraction buffer (Thermo Scientific) supplemented with proteinase (Thermo-Scientific A32953) and phosphatase (Thermo-scientific A32957). Protein was quantified using the Pierce protein assay (Thermo-Scientific #1861426). SDS–polyacrylamide gel electrophoresis was performed using 10% acrylamide gels, and proteins were transferred to nitrocellulose membranes using the Trans-Blot Turbo transfer system (Bio-Rad). Membranes were blocked in 5% milk for 1 hour and incubated overnight at 4°C with primary antibodies with manufacturer-recommended concentrations in 5% bovine serum albumin. After several washes with TBS-T (20 mM Tris (pH 7.6), 140 mM NaCl, and 0.1% Tween 20), blots were incubated with the appropriate HRP-conjugated secondary antibody (Thermo-Fisher Scientific) and imaged using the iBrightCL1000 (Thermo-Fisher). Signals were quantified using ImageJ.

Immunohistochemistry and immunofluorescence

Mouse liver tissues were dissected and placed in 10% buffered formalin overnight at room temperature and dehydrated in a series of graded alcohol. Human HCC specimens were provided by Loyola University Medical Center Pathology Core, and human and mouse liver tissues were paraffin-embedded by the Loyola Pathology Core. Human HCC tissue microarrays were provided by Dr. Robert Lewis and the Mayo Clinic Hepatobiliary SPORE. Tissue blocks were cut into 4 μm sections, dewaxed, and rehydrated. After heat-mediated-citrate-based antigen retrieval, slides were then washed in TBS and blocked using 5% goat serum for 1 h at room temperature before incubation with primary antibodies for 1 hour: Y588 p-EphA2 (1:100), EphA2 (1:200), s473 p-AKT (1:200), p-JAK1 (1:100), p-STAT3 (1:100), AFP (1:200), Ki67 (1:200). Slides were washed in TBST and incubated with biotin-conjugated goat secondary antibody (Thermo Fisher Scientific, depending on the type of species) for 1 hour. Next, slides were incubated with VECTASTAIN® ABC HRP reagent for 30 min at room temperature. Slides were washed in TBST followed by detection by DAB staining for 5 min (Vector Laboratories, SK-4100) for 5 min and finally counterstained with hematoxylin. The IHC signals

were quantified visually. The staining was scored as – (0, negative), + (1, weak signal), + + (2, moderate signal), + + + (3, strong signal) by three independent observers, including a pathologist from Loyola University Chicago, who was masked as to the patient outcome. The average score k was calculated and categorized as negative (k = 0), low (0 < k < 1.5), or high (k > 1.5)

For immunofluorescence, following the incubation with primary antibody and TBST wash, fluorophore-conjugated goat secondary antibody (Thermo Fisher Scientific, depending on the species) was incubated for 1 hour. Slides were then washed in TBST followed by nuclear staining with DAPI mounting media (Vector Laboratories, H-1200)

Transient transfection

PLC/PRF/5 cells were transfected with pT3-EF1α-EphA2 or control pT3-EF1α-GFP plasmids by lipofectamine 3000 (Invitrogen, L3000001) according to the manufacturer's instructions. Forty-eight hours after transfection, total cell lysates were collected used in western blotting.

Lentivirus particle production and transduction

All lentiviral particles were produced in HEK293 cells. The protocol was based on Addgene's lentivirus production protocol with modifications. HEK293 packaging cells were plated onto 10 cm dishes at $3x10^6$ cells for overnight. Two packaging plasmids pCMV-dR8.2 dvpr (Addgene, #8455) pCMV-VSV-G (Addgene, #8454) plus pLKO-based transfer plasmids were diluted in Opti-MEM (GIBCO) with 1 mg/ml PEI at the DNA: PEI ratio of 1:4. Plasmid mixtures were transfected into cells, and the media was replaced with complete DMEM 18 hours after transfection. Lentivirus was harvested 72 hours post-transfection. Collected media was centrifuged at 500 × g for 10 min, and the supernatant was extracted and stored at −80°C. Lentivirus transduction was performed following the Addgene PLKO.1 protocol.

Gene knockdown

Knockdown of *EphA2* in HCC cell lines was performed using lentiviral mediate shRNA expression. pLKO.1-puro-shEphA2-1(CCGGCCATCAAGATGCAGCAGTATACTCGAGTATACTGCTGCATCTTGATGGTTTTTG), pLKO.1-puro-shEphA2-2 (CCGGGATAAGTTTCTATTCTGTCAGCTCGAGCTGACAGAATAGAAACTTATCTTTTTTG), pLKO.1-puro-shEphA2-5 (CCGGTCGGACAGACATATAGGATATCTCGAGATATCCTATATGTCTGTCCGATTTTTG) and scramble control were purchased from Millipore Sigma. Lentiviral particles were produced in HEK293 cells. Cells were selected with puromycin (1 μg/mL).

Knockdown of *JAK1* in HCC cell lines was performed using siRNA. siGENOME SMARTpool siRNA targeting *JAK1* (CCACAUAGCUGAUCUGAAA; UGAAAUCACUCACAUUGUA; UAAGGAACCUCUAUCAUGA; GCAGGUGGCUGUUAAAUCU) was purchased from Dharmacon/Horizon and transfected into HCC cells at a concentration of 100 nM using Lipofectamine RNAiMAX reagent (Thermo-Fisher, #13778075) prepared in OptiMEM (Thermo-Fisher, #31985070) according to manufacturer's protocol. After 48 hours, knockdown efficiency was assessed by western blot.

Cell Viability Assays

HCC cell lines acquired from American Type Culture Collection (ATCC®) or the Japanese Cancer Research Resources Bank (JCRB) were cultured in DMEM or RPMI 1640 supplemented with 10% fetal bovine serum (Tissue Culture Biologicals), 1 × penicillin/streptomycin (Sigma-Aldrich, St. Louis, MO) at 37°C and 5% CO2.

For cell proliferation studies, HCC cells were seeded into 96-well plates (5×10^3 cells/well). At indicated time points, culture media was removed, and alamarBlue (BUF012A; BioRad, Hercules, CA) solution (1:10 dilution in DMEM) was added to the cells. After a 4-hours-incubation at 37°C, fluorescence values were measured with a fluorescent plate reader at 530-560 nm excitation/590 nm emission.

For IC_{50} of ALW-II-41-27(ALW) studies, HCC cells were seeded into 96-well plates (5×10^3 cells/well). After 24 hours, cells were treated with 0, 0,25, 0.5, 1, 2, or 4 μM of ALW. After 48 hours, culture media was removed, and alamarBlue (BUF012A; BioRad, Hercules, CA) solution (1:10 dilution in DMEM) was added to the cells. After 4 hours of incubation at 37°C, fluorescence values were measured with a fluorescent plate reader at 530-560 nm excitation/590 nm emission.

For IC_{50} of MK-2206 and BBI608 studies, HCC cells were seeded into 96-well plates (5×10^3 cells/well). After 24 hours, cells were treated with different doses (0-10 μM) of MK-2206 (S1078, Selleck chemicals) or BBI608 (S7977, Selleck chemicals). According to the manufacturer's instructions, after 48 hours, cell viability was measured with CCK-8 kit (Dojindo, CK04).

High-resolution hepatic ultrasound

Hepatic ultrasound was performed using micro-ultrasound system (Vevo 2100, Visualsonics) with 40 MHz ultrasound transducer (MS550D, Visualsonics) by the Small Animal Core Facility at Loyola University Chicago Health Sciences Division.

RNA isolation, RNA sequencing, dataset analysis, and qPCR

All total RNA was extracted using the RNeasy Plus Mini Kit (QIAGEN) following the manufacturer's protocol. RNA-seq was performed by Novogene Corporation and analyzed by Dr. Jun Li from the University of Notre Dame. Gene set enrichment analysis was performed using GSEA software (Broad MIT, http://www.gsea-msigdb.org/gsea/index.jsp). A detailed user guide can be found from https://www.gsea-msigdb.org/gsea/doc/GSEAUserGuideFrame.html. In brief, expression database files were prepared, and data

files were then loaded into GSEA. The analysis parameters (Hosted MSigDB Gene Sets, H1, and C6) were set, and analysis was run as the user guide indicated.

All RNA expression data from The Cancer Genome Atlas Liver Hepatocellular Carcinoma cohort was analyzed using Gene Expression Profiling Interactive Analysis (GEPIA) (Tang et al., 2017). The data of GSE14520 was retrieved from the Gene Expression Omnibus (https://www.ncbi.nlm.nih.gov/geo/query/acc.cgi?acc=gse14520). To create the Kaplan-Meier plots, Python 3.0 was used to analyze the original data. Specifically, censored data was generated by dividing patients into two groups. The censored group consisted of patients who had not experienced death by the end of the study time. Patient data was also separated into two groups based on the expression level indicated by expression values (mean of 25% top versus 25% bottom). Binary censored data, binary expression group data, and survival times were imported into R 3.6.0. Kaplan-Meier plots were created using survival, survminer, dplyr packages, Surv, survfit, and ggsurvplot functions. *P*-values were generated by including the command "pval = TRUE" in the ggsurvplot function from the survminer library. Hazard ratios for 3 years survival were analyzed based on the median cutoff, and the p value is for the effect of each dichotomized gene in univariable Cox proportional hazards analysis.

For qPCR, 1 μg of RNA was reverse transcribed with iScript cDNA Synthesis Kit (Bio-Rad). qRT-PCR was performed with iTaq Universal SYBR Green Supermix (Bio-Rad) on the Real-Time PCR System. Primer pairs were selected from the Primer Bank (https://pga.mgh.harvard.edu/primerbank/) (Table S3B). Relative expression values for each gene of interest were obtained by normalizing to GAPDH mRNA expression using the $\Delta\Delta C_t$ method.

Proximity Ligation Assay

Proximity ligation assay (PLA) was performed using the Duolink® *In Situ* Red Starter Kit Mouse/Rabbit (Millipore Sigma) according to the manufacturer's instructions. In brief, cells were seeded on an 8 well-Nunc Lab-Tek II CC2 Chamber Slide System (Thermo Fisher) at $17.5x10^3$/well overnight, then fixed with 4% paraformaldehyde for 30 min at room temperature and washed in PBS, followed by permeabilization with 0.1% Triton X-100 for 10 min. After washing with Wash Buffer A (Millipore Sigma) followed by blocking with Duolink Blocking Buffer (Millipore Sigma) for 30 min at room temperature, cells were incubated with primary antibodies (EphA2, 1:200 Santa Cruz and JAK1, 1:100, Cell Signaling) overnight at 4°C. The next day, cells were washed repeatedly in Wash Buffer A, followed by incubation with appropriate Duolink secondary antibodies (Millipore Sigma) for 1 hour at 37°C according to the manufacturer's protocol. After washing with Wash Buffer A at room temperature, ligation, and amplification steps of the PLA were performed according to the manufacturer's protocol. After final washes with Wash Buffer B at room temperature, slides were mounted with Corning® 24x50 mm Rectangular #1 Cover Glass (Corning) using Duolink® *In Situ* Mounting Medium with DAPI (Millipore Sigma).

EFNA1-FC experiment

The stock solution of Recombinant Human Ephrin-A1 Fc Chimera Protein (R&D Systems; EFNA1-Fc) was prepared in PBS at 100 μg/mL and diluted to 0.1 μg/mL in DMEM based culture medium. After HCC cells were seeded in a 6-well-culture plate $1.7x10^5$/well overnight, the medium was removed, and the cells were treated with 0.1 μg/mL EFNA1-Fc for 0, 2, 4, 8, 12, 16, 24, or 32 hours. Cell lysates were collected at these experimental times and analyzed by western blot.

IL6 ELISA analysis

The culture supernatants from the scrambled and EphA2 knockdown Huh7 cells were collected, and IL-6 protein levels were measured using Human IL-6 ELISA Kit (RAB0306, Sigma-Aldrich), according to the manufacturer's instructions.

QUANTIFICATION AND STATISTICAL ANALYSIS

Statistical tests used are indicated in the figure legends. Student's t test (unpaired, two-tailed) was used to assess significance between experiment and control groups. One-way ANOVA was used to determine if there is statistical significance between multiple experiment groups. The log-rank test was used to assess the significance of differences in survival between the control and *EphA2* knockout group. Chi-square test was used to determine the significance of correlations in TMAs. $p < 0.05$ was considered significant. plots and statistical analyses were done using Prism version 7 software (GraphPad) and Excel.

Cell Reports, Volume *34*

Supplemental information

Targeting EphA2 suppresses hepatocellular carcinoma initiation and progression by dual inhibition of JAK1/STAT3 and AKT signaling

Hao Wang, Wei Hou, Aldeb Perera, Carlee Bettler, Jordan R. Beach, Xianzhong Ding, Jun Li, Mitchell F. Denning, Asha Dhanarajan, Scott J. Cotler, Cara Joyce, Jun Yin, Fowsiyo Ahmed, Lewis R. Roberts, and Wei Qiu

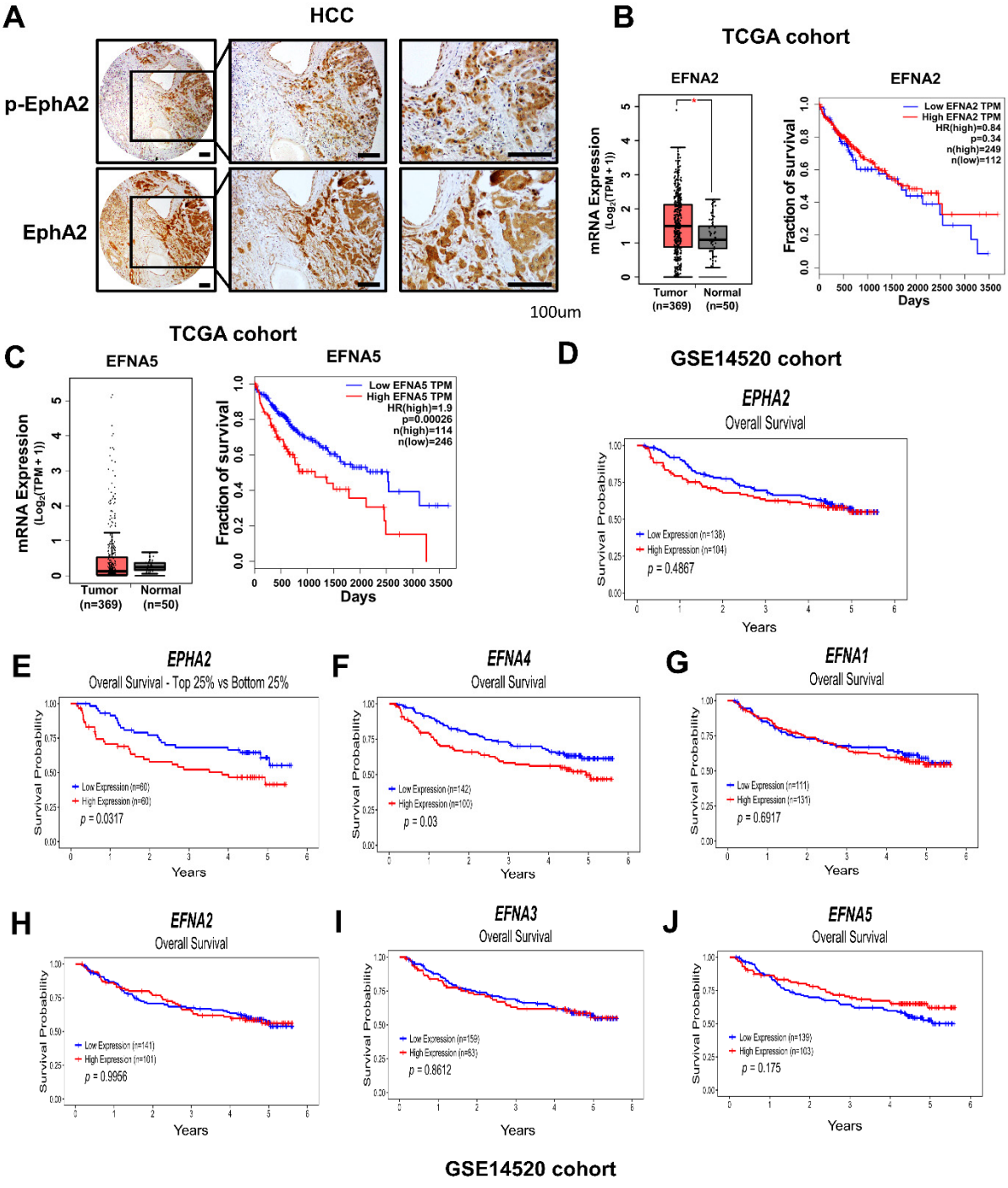
A
HCC
p-EphA2
EphA2
100um
B
TCGA cohort
EFNA2
mRNA Expression
Tumor (n=369)
Normal (n=50)
EFNA2
Low EFNA2 TPM
High EFNA2 TPM
HR(high)=0.84
p=0.34
n(high)=249
n(low)=112
Fraction of survival
Days
C
TCGA cohort
EFNA5
mRNA Expression
Tumor (n=369)
Normal (n=50)
EFNA5
Low EFNA5 TPM
High EFNA5 TPM
HR(high)=1.9
p=0.00026
n(high)=114
n(low)=246
Fraction of survival
Days
D
GSE14520 cohort
EPHA2
Overall Survival
Survival Probability
Low Expression (n=138)
High Expression (n=104)
p = 0.4867
Years
E
EPHA2
Overall Survival - Top 25% vs Bottom 25%
Survival Probability
Low Expression (n=60)
High Expression (n=60)
p = 0.0317
Years
F
EFNA4
Overall Survival
Survival Probability
Low Expression (n=142)
High Expression (n=100)
p = 0.03
Years
G
EFNA1
Overall Survival
Survival Probability
Low Expression (n=111)
High Expression (n=131)
p = 0.6917
Years
H
EFNA2
Overall Survival
Survival Probability
Low Expression (n=141)
High Expression (n=101)
p = 0.9956
Years
I
EFNA3
Overall Survival
Survival Probability
Low Expression (n=159)
High Expression (n=83)
p = 0.8612
Years
J
EFNA5
Overall Survival
Survival Probability
Low Expression (n=139)
High Expression (n=103)
p = 0.175
Years
GSE14520 cohort

Figure S1. EphA2 and its ligands expression in HCC and their correlation with overall survival. Related to Figure 1.

(A) Representative immunohistochemistry (IHC) images of Y588 p-EphA2 and total EphA2 in HCC tissue microarray. Scale bars, 100 μm.
(B) Left, a boxplot of relative mRNA expression levels of EFNA2 comparing normal vs. HCC tissue. Right, Kaplan-Meier plot of overall survival of HCC patients stratified by EFNA2 expression levels. Data from TCGA (GEPIA).
(C) Left, a boxplot of relative mRNA expression levels of EFNA5 comparing normal vs. HCC tissue. Right, Kaplan-Meier plot of overall survival of HCC patients stratified by EFNA5 expression levels. Data from TCGA (GEPIA).
(D-J) Kaplan-Meier plot of overall survival of HCC patients stratified by EphA2 and its ligands expression levels. Data from NCBI GEO (GSE14520). Statistical significance was determined by log-rank test for Kaplan-Meier plot.

Statistical significance was determined by two-tailed Student's t-test *$p < 0.0001$ for boxplots and log-rank test for Kaplan-Meier plot.

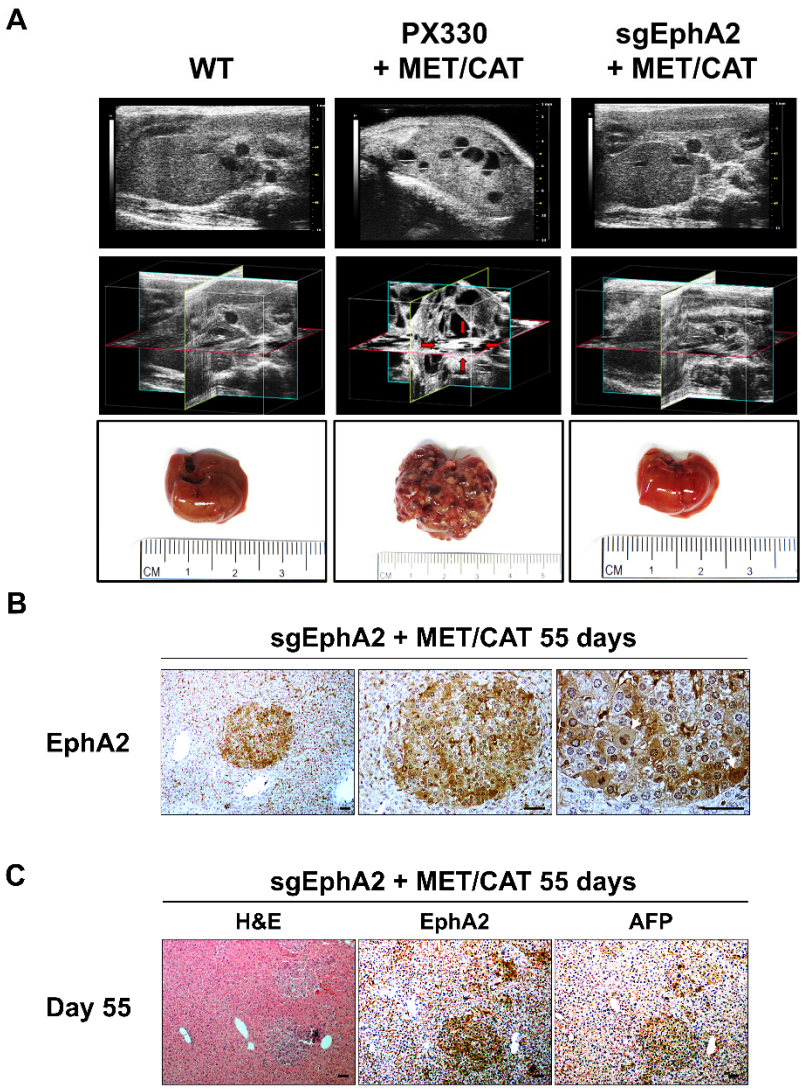

Figure S2. EphA2 knockout delays MET/CAT-induced HCC, and escape from EphA2 deletion reinitiate tumor growth in MET/CAT induced HCC. Related to Figure 3.

(A) Top, representative 2D liver ultrasound images of wild type mice (untreated), PX330, and sgEphA2 injected MET/CAT mice 55 days after injection. Middle, 3D reconstruction mice liver. Prominent hyperechoic tumor mass (red arrow) surrounded by necrotic and hemorrhagic cysts. Bottom, gross representation of the mice livers.

(B) The liver of sgEphA2 MET/CAT mice was extracted 55 days after injection and immunohistochemically assessed for total EphA2 expression. There are multiple microscopic foci of dysplastic hepatocyte nodules stained positive for EphA2. On the other hand, the non-dysplastic background liver hepatocytes are negative for EphA2. Notably, the dysplastic foci are associated with strong EphA2 expression characterized by nuclear crowding, enlarged hyperchromatic nucleus, and frequent mitotic bodies (white arrows) consistent with early HCC. Scale bar, 50 μm.

(C) The liver of sgEphA2 MET/CAT mice described in (A) was collected for H&E and immunohistochemistry for EphA2 and AFP (HCC marker). Scale bar, 50 μm.

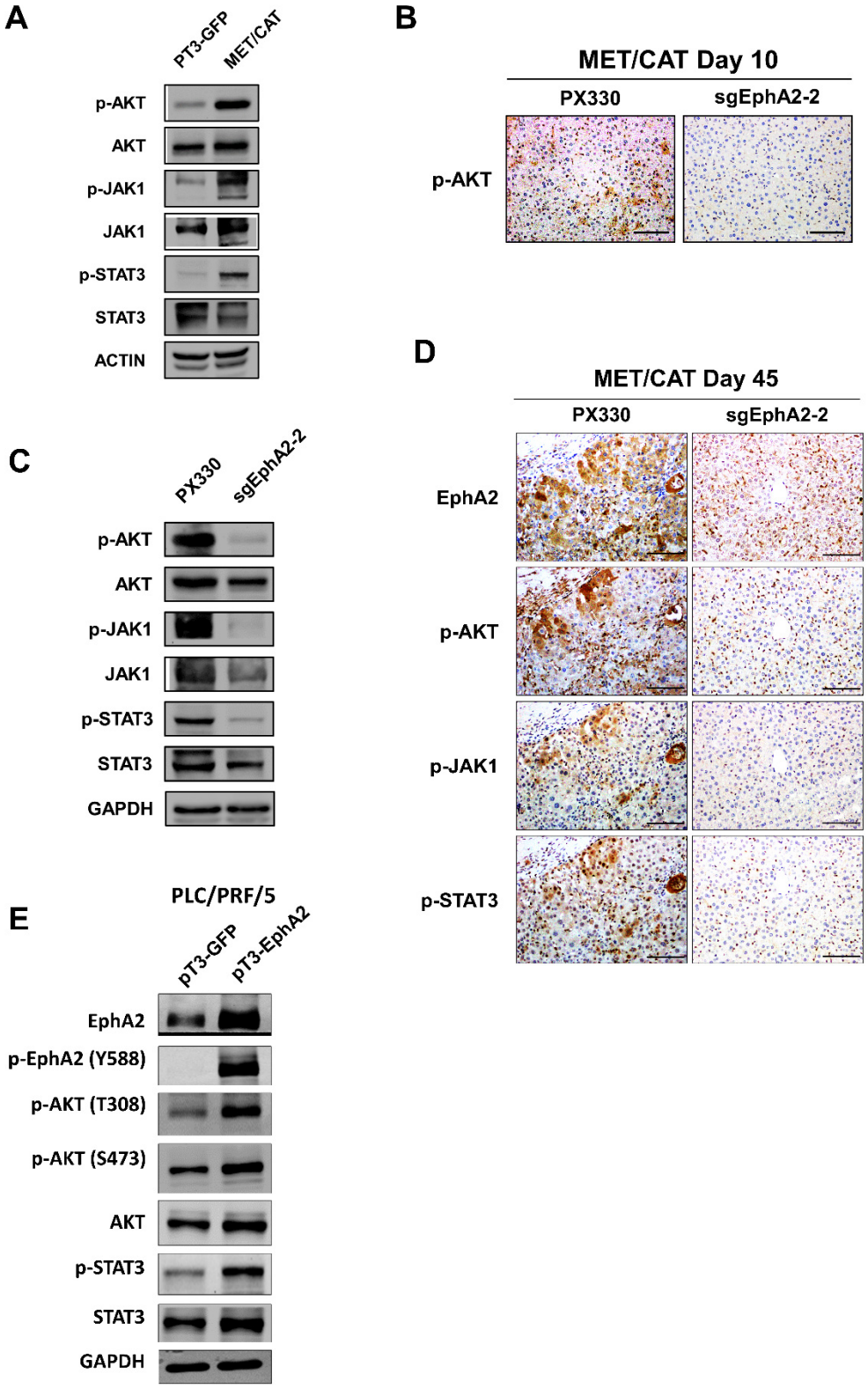
A
PT3-GFP
MET/CAT
p-AKT
AKT
p-JAK1
JAK1
p-STAT3
STAT3
ACTIN
B
MET/CAT Day 10
PX330
sgEphA2-2
p-AKT
C
PX330
sgEphA2-2
p-AKT
AKT
p-JAK1
JAK1
p-STAT3
STAT3
GAPDH
D
MET/CAT Day 45
PX330
sgEphA2-2
EphA2
p-AKT
p-JAK1
p-STAT3
E
PLC/PRF/5
pT3-GFP
pT3-EphA2
EphA2
p-EphA2 (Y588)
p-AKT (T308)
p-AKT (S473)
AKT
p-STAT3
STAT3
GAPDH

Figure S3. Loss of EphA2 inhibits AKT and JAK1/STAT3 activity in MET/CAT induced HCC, and overexpression of EphA2 in HCC cells increases both AKT and STAT3 signaling. Related to Figures 3, 4, 5, and 6.

(A) Western blot analysis of indicated proteins from GFP (PT3-GFP) or MET/CAT mouse liver seven weeks after injection. ACTIN as a loading control.
(B) Liver of EphA2 knockout MET/CAT mice was extracted and immunohistochemically assessed for p-AKT expression comparing to control (PX330). Scale bar, 100 μm.
(C) Western blot analysis of indicated proteins from MET/CAT liver ten days after injection with empty vector (PX330) or sgEphA2. GAPDH as a loading control.
(D) Livers of MET/CAT mice injected with PX330, or sgEphA2 were collected at day 45 and immunohistochemically assessed for EphA2, p-AKT, p-JAK1, and p-STAT3. Scale bars, 100 μm.
(E) Western blot analysis of indicated proteins in PLC/PRF/5 cells transfected with pT3-GFP or pT3-EphA2 for 48 hours. GAPDH as a loading control.

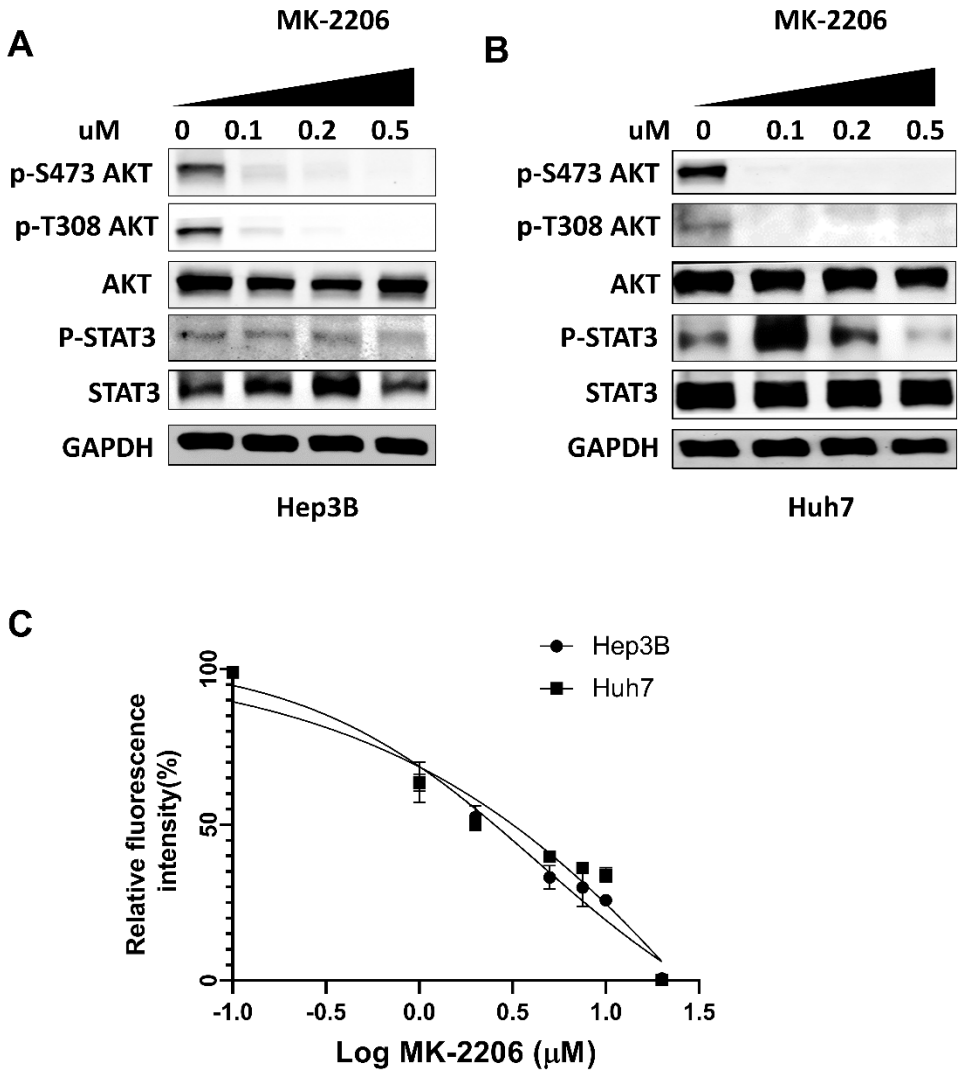

Fig. S4. AKT inhibitor MK2206 suppresses HCC cell growth but not STAT3 activity. Related to Figures 4 and 5.

(A) Western blot analysis of indicated proteins at the selected concentration of MK-2206 for 24 hours in Huh7 cells. GAPDH as a loading control.

(B) Western blot analysis of indicated proteins at the selected concentration of MK-2206 for 24 hours in Hep3B cells. GAPDH as a loading control.

(C) The effect of MK-2206 on Huh7 and Hep3B cells' proliferation was assessed after 48 hours of treatment using CCK-8 assay. Values are mean± SD (n=3).

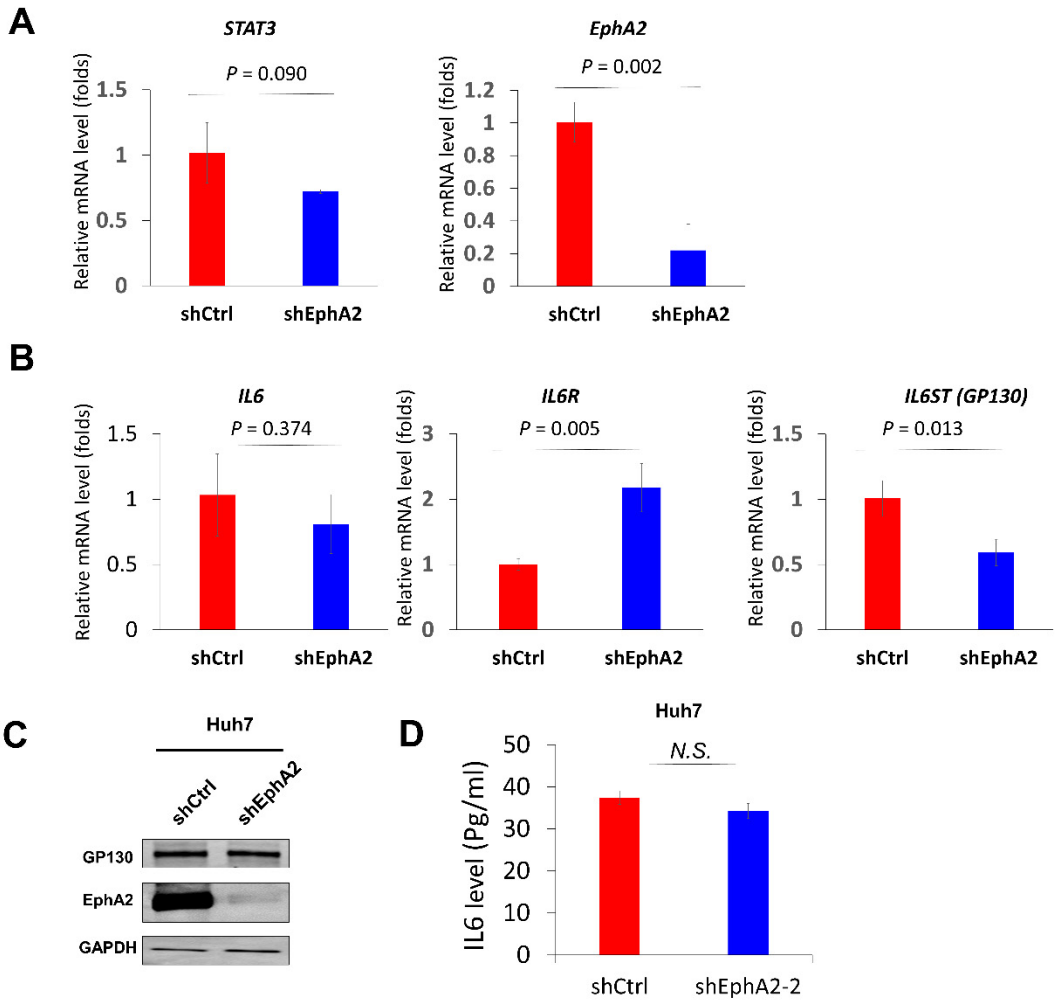

Fig. S5. EphA2 knockdown does not affect the expression and secretion of IL6 in HCC cells. Related to Figures 5.

(A) Real-time PCR analysis of *STAT3* and *EphA2* in scrambled and EphA2 knockdown Huh7 cells. GAPDH was used as an internal control.
(B) Real-time PCR analysis of indicated genes in scrambled and EphA2 knockdown Huh7 cells. GAPDH was used as an internal control.
(C) Cell lysate of scrambled and EphA2 knockdown Huh7 cells was immunoblotted for GP130, EphA2, and GAPDH.
(D) The culture supernatants from the scrambled and EphA2 knockdown Huh7 cells were collected, and IL-6 protein levels were measured using Human IL-6 ELISA Kit.

Statistical significance was determined by a two-tailed Student t-test (A, B,&D). N.S., not significant.

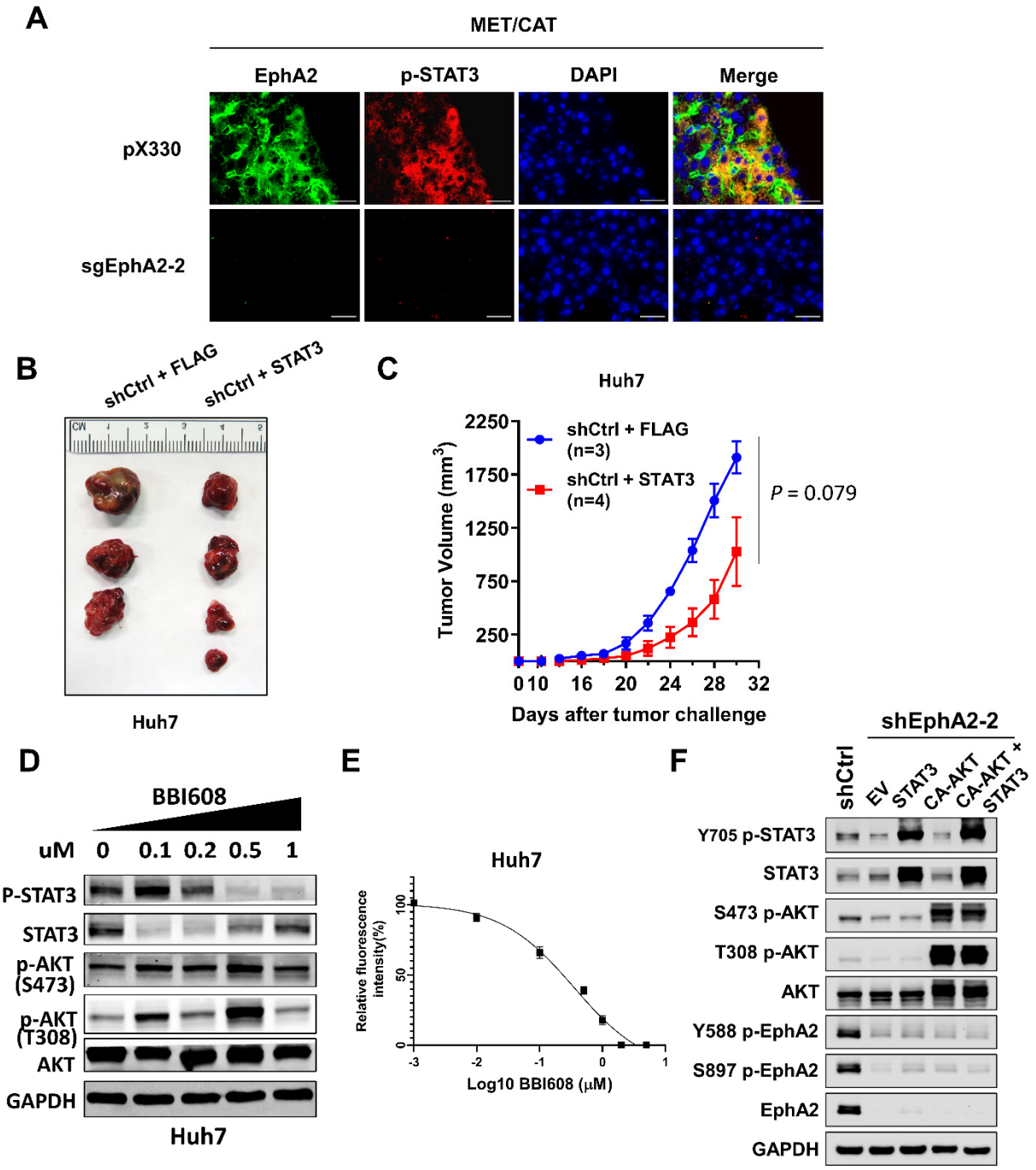
A
MET/CAT
EphA2
p-STAT3
DAPI
Merge
pX330
sgEphA2-2
B
shCtrl + FLAG
shCtrl + STAT3
Huh7
C
Huh7
shCtrl + FLAG (n=3)
shCtrl + STAT3 (n=4)
P = 0.079
Tumor Volume (mm3)
2250
1750
1250
750
250
0 10 16 20 24 28 32
Days after tumor challenge
D
BBI608
uM 0 0.1 0.2 0.5 1
P-STAT3
STAT3
p-AKT (S473)
p-AKT (T308)
AKT
GAPDH
Huh7
E
Huh7
Relative fluorescence intensity(%)
100
50
0
-3 -2 -1 0 1
Log10 BBI608 (μM)
F
shEphA2-2
shCtrl
EV
STAT3
CA-AKT
CA-AKT + STAT3
Y705 p-STAT3
STAT3
S473 p-AKT
T308 p-AKT
AKT
Y588 p-EphA2
S897 p-EphA2
EphA2
GAPDH

Fig. S6 EphA2 promotes tumor development partially through activation of STAT3 signaling. Related to Figures 5.

(A) Immunofluorescence analysis of EphA2 and p-STAT3 in MET/CAT model 10 days after injection. EphA2 (green), p-STAT3 (red). Nuclei were stained with DAPI (blue). Scale bars, 30 μm
(B) Representative picture of tumors extracted from NSG-A2 mice 30 days after subcutaneous injection with Huh7 cells as described. N=3 or 4 mice in each group.
(C) Primary tumor size from the mice (B) was recorded every two days. Values are mean± SEM.
(D) Western blot analysis of indicated proteins at the selected concentration of BBI608 for 24 hours in Huh7 cells. GAPDH as a loading control.
(E) The effect of BBI608 on cell proliferation of Huh7 cells was assessed after 48 hours of treatment using CCK-8 assay. Values are mean± SD (n=3).
(F) Western blot analysis of indicated proteins in Huh7 scrambled or EphA2 knockdown cells overexpressed with control (EV), AKT, STAT3, or both. GAPDH as a loading control.

A

	Normalized Expression Levels					
Gene Symbol	shCtrl_1	shCtrl_2	shCtrl_3	shEphA2_2_1	shEphA2_2_2	shEphA2_2_3
JAK1	2508.6316	2547.8344	2461.9476	2319.1578	2471.3773	2430.0674
JAK2	179.371	157.2378	167.5622	101.0915	165.4522	111.7884
JAK3	5.979	7.7648	2.8083	11.8931	5.2029	7.9849

B

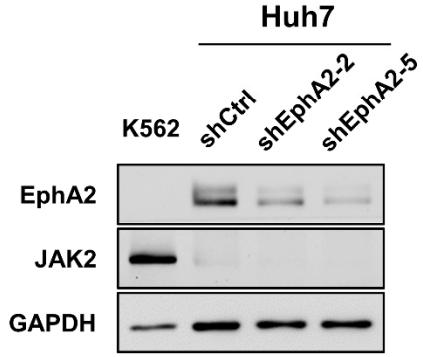

C

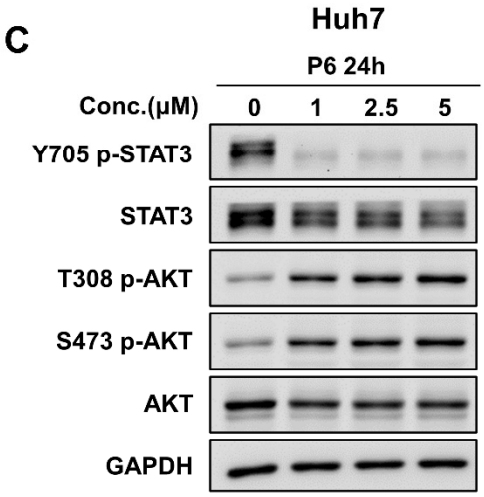

D

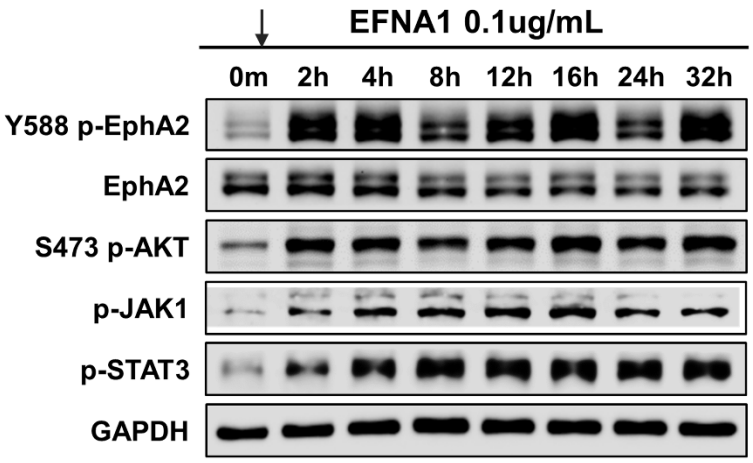

Figure S7. JAK1 is an intermediate of EphA2/STAT3 signaling, and recombinant EFNA1-Fc activates EphA2 signaling and its downstream effectors AKT and JAK1/STAT3 in HCC. Related to Figure 6.

(A) Normalize RNA expression of JAK1, JAK2, and JAK3 in scramble (shCtrl) or *EphA2* knockdown Huh7 cell.
(B) Western blot confirmation of JAK2 expression in Huh7 cells. K562 as a positive control. GAPDH as a loading control.
(C) Western blot analysis of indicated protein from Huh7 cells treated with JAK inhibitor (pyridine 6, P6) for 24 hours. GAPDH as a loading control.
(D) Cell lysates of Huh7 treated with 0.1 μg/mL of EFNA-Fc at indicated times were immunoblotted for Y588 p-EphA2, EphA2, p-JAK1, p-STAT3, and p-AKT. GAPDH as a loading control.

EphA2 IHC Score	0 (n=16)	1 (n=91)	2 (n=32)	3 (n=14)	Total (n=153)	*p* value
Age						0.097
Mean (SD)	62.4 (13.1)	63.9 (13.4)	64.0 (14.0)	53.8 (19.6)	62.8 (14.3)	
Median	64.0	66.0	67.0	62.5	66.0	
Range	32.0 - 79.0	28.0 - 96.0	20.0 - 85.0	23.0 - 77.0	20.0 - 96.0	
Gender						0.614
F	6 (37.5%)	34 (37.8%)	13 (41.9%)	3 (21.4%)	56 (37.1%)	
M	10 (62.5%)	56 (62.2%)	18 (58.1%)	11 (78.6%)	95 (62.9%)	
Race						0.018
Asian	1 (7.7%)	3 (4.2%)	0 (0.0%)	0 (0.0%)	4 (3.2%)	
African American	0 (0.0%)	1 (1.4%)	1 (3.7%)	2 (16.7%)	4 (3.2%)	
Other	0 (0.0%)	6 (8.3%)	0 (0.0%)	0 (0.0%)	6 (4.8%)	
White	12 (92.3%)	62 (86.1%)	26 (96.3%)	9 (75.0%)	109 (87.9%)	
Hepatitis B	1 (6.7%)	13 (15.3%)	2 (7.4%)	4 (28.6%)	20 (14.2%)	0.462
Hepatitis C	2 (13.3%)	20 (23.8%)	7 (25.9%)	2 (14.3%)	31 (22.1%)	0.736
Alcohol Abuse	3 (18.8%)	27 (30.7%)	7 (24.1%)	4 (28.6%)	41 (27.9%)	0.800
Cancer Stage						0.932
T Stage						0.562
N Stage						0.615
M Stage						0.891
No. of Tumors						0.803
One	9 (60.0%)	64 (70.3%)	23 (74.2%)	10 (71.4%)	106 (70.2%)	
Multiple	6 (40.0%)	27 (29.7%)	8 (25.8%)	4 (28.6%)	45 (29.8%)	
Primary Or Metastatic						0.307
metastatic	1 (6.2%)	1 (1.1%)	0 (0.0%)	0 (0.0%)	2 (1.3%)	
primary	15 (93.8%)	89 (98.9%)	31 (100.0%)	14 (100.0%)	149 (98.7%)	

Table S1. TMA Patient characteristics. Related to Figure 1.

Gene	Mean (SD)	Hazard ratio (95% CI) for 1 SD increase	*p*-value
EphA2	4.56 (0.63)	1.31 (1.08-1.57)	0.005
EFNA1	9.50 (0.96)	1.17 (0.92-1.48)	0.20
EFNA2	3.57 (0.22)	1.00 (0.80-1.25)	0.99
EFNA3	4.38 (0.64)	1.13 (0.93-1.38)	0.20
EFNA4	4.29 (0.57)	1.47 (1.21-1.80)	<0.001
EFNA5	3.48 (0.24)	0.84 (0.64-1.11)	0.23

Table S2. Hazard ratios for 3-year survival of the GSE14520 cohort. Related to Figure 1.

A

NAME	NES	*p*-value
MYOGENESIS	-2.0354	0
JAK_STAT3_SIGNALING	-1.9501	0
ERBB2_UP.V1_UP	-1.8854	0
ESTROGEN_RESPONSE-LATE	-1.8029	0
KRAS_SIGNALING_UP	-1.6024	0.0035757
ANGIOGENSIS	-1.572	0.0226897
AKT_UP.V1_UP	-1.5162	0.0095465
CYCLIN_D1_UP.V1_UP	-1.4969	0.0035928
COAGULATION	-1.4911	0.0139417
KRAS.BREAST_UP.V1_UP	-1.4856	0.0227848

B

Species	Gene	FW (5' 3')	RV (5' 3')
human	*EphA2*	TGGCTCACACACCCGTATG	GTCGCCAGACATCACGTTG
human	*NANOG*	TTTGTGGGCCTGAAGAAAACT	AGGGCTGTCCTGAATAAGCAG
human	*SOX2*	GCCGAGTGGAAACTTTTGTCG	GGCAGCGTGTACTTATCCTTCT
human	*KLF4*	CCCACATGAAGCGACTTCCC	CAGGTCCAGGAGATCGTTGAA
human	*EPCAM*	AATCGTCAATGCCAGTGTACTT	TCTCATCGCAGTCAGGATCATAA
human	*CD90*	ATGAAGGTCCTCTACTTATCCGC	GCACTGTGACGTTCTGGGA
human	*HIF1a*	GAACGTCGAAAAGAAAAGTCTCG	CCTTATCAAGATGCGAACTCACA
human	*TGFb1*	CTCCCGTGGCTTCTAGTGC	GCCTTAGTTTGGACAGGATCTG
human	*STAT3*	CAGCAGCTTGACACACGGTA	AAACACCAAAGTGGCATGTGA
human	*IL6*	ACTCACCTCTTCAGAACGAATTG	CCATCTTTGGAAGGTTCAGGTTG
human	*IL6R*	CCCCTCAGCAATGTTGTTTGT	CTCCGGGACTGCTAACTGG
human	*IL6ST*	CGGACAGCTTGAACAGAATGT	ACCATCCCACTCACACCTCA

Table S3. Enriched gene sets affected by EphA2 knockdown in Huh7 cells (A) and primer sequences for RT-qPCR (B). Related to Figures 4, 5, S5, and STAR Methods.